Quasiclassical Trajectory Binning: A Systematic Study of the Effect of Binning on Li_2 + Ne Scattering

by

Christopher Roth
Class of 2015

A thesis submitted to the
faculty of Wesleyan University
in partial fulfillment of the requirements for the
Degree of Bachelor of Arts
with Departmental Honors in Physics

"Stupidity is 1% (put synonym for stupid here) and 99% procrastination."

Abstract

Although quantum mechanics is the most accurate descriptor of nature at molecular length scales, sophisticated quantum calculations are still infeasible for complex systems. As a result, there is a demand for methods of classical calculation that are able to accurately simulate systems with quantum features. In this study, we examine modifications to the quasiclassical trajectory method (QCT) on the Li_2 + Ne inelastic scattering system. More specifically, we examine the effects of binning, the process of discretizing the continuous distribution of final classical actions in order to calculate collision cross sections for rovibrational transitions. In order to undertake this, we calculate collision cross sections using the QCT with a variety of different binning methods. We examine the efficacy of these binning methods through comparing the QCT results with quantum mechanical results, and through testing the QCT for time reversal symmetry.

Acknowledgements

Thanks to Professor Stewart for two and a half years of great research, and for pushing me towards the finish line. Thanks to Tess for all the support. Thanks to Nick for always making me feel like I'm ahead on my thesis. Thanks to the rest of 30 fountain for the "I haven't started my thesis yet" joke. Thanks to my homies at 107 cross, 35 fountain, 113 cross, and the rest of keg coop. Thanks to taco coop. Thanks to my family for their unwavering support ...

Contents

Chapter 1

Binning and The Quasiclassical Trajectory Method

1.1 Introduction

Although quantum mechanics is the most accurate descriptor of nature at small length scales, it only yields analytic solutions for very simple problems. Furthermore, it is often computationally prohibitive to simulate complex systems with quantum mechanics, as the computation time scales with the number of channels cubed. In order to address this issue, one either has to resort to an approximate treatment, or use classical mechanics to simulate the system. For many channel systems, a non-approximate classical treatment often provides the most accurate way to simulate a system under reasonable time constraints. Additionally, classical treatments are

valuable because they can provide a more intuitive description of dynamics, as classical processes dominate the macroscopic scale. As a result, there is a high demand for methods of classical calculation that are able to provide a good representation of systems with quantum features.

Since it is impossible to find an analytical solution for most systems involving three or more bodies, many body systems are often modeled using statistical methods. The dominant classical statistical method is called the quasiclassical trajectory method, which describes the behavior of a collision system through analyzing the dynamics on a case by case basis. **In this report we attempt to improve upon the quasiclassical treatment of atom-diatom scattering systems, through examining techniques that incorporate features of the quantum description into the classical one.**

1.2 Our Choice of System

Our study focuses on rovibrational energy transfer in the non-reactive scattering system

$$\mathrm{Li}_2(v_i,\ j_i) + \mathrm{Ne} \rightarrow \mathrm{Li}_2(v_f,\ j_f) + \mathrm{Ne}, \tag{1.1}$$

where (v_i, j_i) are the initial rotational and vibrational quantum numbers, and (v_f, j_f) are the final rotational and vibrational quantum numbers.

While there have been many studies on the effect of novel quasiclassical techniques on reactive systems [Banares et al. [1], Balucani et al. [2, 3], Czakó and Bowman

[4]], there have been far fewer that mention inelastic scattering [Díaz et al. [5]], and **none to our knowledge study rovibrationally inelastic scattering in a three-dimensional three-body system**. We believe that a comprehensive study, which examines the applicability of recent advances in the field of quasiclassical simulations to pure inelastic scattering, will be useful to others who wish to use classical calculations on scattering systems. We hope that through doing classical calculations on this **relatively simple three-body system**, and comparing the results to those obtained from quantum mechanics, we can provide insight into the reasons that classical and quantum mechanics diverge.

Finally, through testing a wide variety of quasiclassical trajectory method variants against one-another, we hope to put forth a prescription that describes how to best make classical calculations agree with quantum mechanics.

1.3 Method of Classical Calculation: The quasiclassical Trajectory Method

In order to describe the dynamics of the $Li_2 + Ne$ system, we use a tool called the quasiclassical trajectory method (QCT), which uses classical mechanics to simulate the system on a case-by case basis. For a batch of trajectories, we specify the collision energy and the initial rovibrational state (v_i, j_i), and randomize the rest of the initial conditions using Monte-Carlo sampling. After running an enormous amount of trajectories, typically of order 10^8, we are able to gain insight into the bulk behavior of the collisions, averaged over the initial conditions. We analyze a quantity

called the collision-cross section, which gives the effective area, perpendicular to the relative velocity of the atom with respect to the diatom, over which a given transition is excited within the molecule. If the trajectories are sampled equally over a perpendicular area, πb_{max}^2 that encompasses all collisions that cause the transition $(v_i, j_i) \rightarrow (v_f, j_f)$, the collision cross section can be calculated using the following equation [Gentry [6]]

$$\sigma(v_i, j_i \rightarrow v_f, j_f) = \pi b_{max}^2 \lim_{N \rightarrow \infty} \frac{n_{v_f, j_f}}{N}. \tag{1.2}$$

Here n_{v_f,j_f} is the **effective number of classical trajectories** that are said to have made the transition from the state (v_i, j_i) to the state (v_f, j_f), and N is the total number of trajectories. As we will discuss later, calculating n_{v_f,j_f} from the distribution of final classical states is one of the major difficulties associated with the implementation of the quasiclassical trajectory method.

In order to simulate the classical evolution of a three-body system, a number of initial conditions must be selected. While the three-dimensional Li_2 + Ne scattering system has eighteen phase space degrees of freedom, ten of these can be ignored through a suitable transformation of coordinates. This leaves eight parameters that are necessary to define a unique system. Typically, three are kept constant for a batch of trajectories; the initial rotational and vibrational actions, v_i and j_i, which are set to equal to the initial quantum numbers, and the collision energy. Four others, related to the initial state of the diatomic molecule, are randomized to reflect the probability distribution of molecular orientations that the atom sees as it approaches. Finally the impact parameter, b, which represents the distance of closest approach between

the atom and the molecule, should be sampled over a discrete range $b < b_{max}$, in such a way that the atom lands in every place with equal probability on the disk drawn out by rotating b_{max} by 2π. However, we do not sample in such a way, as this would force our trajectory program to calculate a lot of trajectories with high impact parameters. Since high impact parameter trajectories are less likely to cause interesting dynamics, we can improve our signal to noise by sampling them less frequently. To do this, we utilize a trick to improve the signal to noise ratio. Instead of sampling the impact parameter linearly, as would be required to sample evenly over a disk, we sample the impact parameter equally throughout the range of b_{max}. In order to restore uniform sampling, we weight the contribution of the final trajectories to the cross section by their impact parameter [Gentry [6]]. Sampling uniformly in b, we instead calculate the collision cross section as follows,

$$\sigma(v_i, j_i \rightarrow v_f, j_f) = 2\pi b \; b_{max} \lim_{N\rightarrow\infty} \frac{n_{v_f,j_f}}{N}. \tag{1.3}$$

After choosing the initial conditions, we can use either of two common methods to simulate the collision dynamics. One involves converting the initial conditions into cartesian coordinates and integrating over Hamilton's equations of motion [Burgess [7]]. We choose to implement the other one, which integrates over the equations of motion in action-angle coordinates [Smith [8]]. **This method has the advantage of directly calculating the classical actions, the classical correlate of the quantum numbers.** As a potential energy function, we use the Li_2 + Ne *ab initio* potential energy surface constructed by Alexander and Werner [Alexander et al. [9]].

However, the action distribution that emerges from a classical calculation is continuous, as classical mechanics does not contain a quantization constraint. **As a result, in order to calculate collision cross sections, we must discretize this continuous distribution of classical actions at the allowed rovibrational quantum numbers.** This process of figuring out how to best convert this continuum of classical actions into a discrete set of quantum numbers is known as **binning**, and it will be the focus of our study.

1.4 The Classical Cross Section

In order to avoid this dilemma temporarily, we introduce $\frac{\partial^2\sigma}{\partial v_c\ \partial j_c}$, the classical differential cross section [Stewart et al. [10]], where v_c is the continuous final vibrational classical action and j_c is the continuous final rotational classical action. In order to calculate the classical differential cross section, we take the derivative of Equation 1.2 with respect to the rotational and vibrational actions from the trajectory data

$$\frac{\partial^2\sigma}{\partial v_c\ \partial j_c}(v_c, j_c) = \pi b_{max}^2 \lim_{N\to\infty} \frac{1}{N} \frac{\partial^2 n}{\partial v_c \partial j_c}. \tag{1.4}$$

While the nature of the quantity n_{eff} in Equation 1.2 was difficult to describe classically, the quantity $\frac{\partial^2 n}{\partial v_c, \partial j_c}$ is just the density distribution of trajectories in classical rovibrational phase space. Therefore, the classical cross section can be calculated as follows

$$\frac{\partial^2\sigma}{\partial v_c\ \partial j_c}(v_c, j_c) = \pi b_{max}^2 \lim_{N\to\infty} \frac{\rho(v_c, j_c)}{N}, \tag{1.5}$$

where $\rho(v_c, j_c)$ is this density distribution. While the traditional collision cross section only exists for transitions between quantum states, this classical differential cross section is defined throughout rovibrational phase space.

The classical differential cross sections can be calculated by counting the number of trajectories that land in the range $[(v_c - \frac{\Delta v_c}{2}, v_c + \frac{\Delta v_c}{2}), (j_c - \frac{\Delta j_c}{2}, j_c + \frac{\Delta j_c}{2})]$ and multiplying by $\frac{\pi b_{max}^2}{N}$, for a variety of classical actions spaced by Δv in vibrational space and Δj in rotational space. The rest of the function can be interpolated by connecting these points with linear fits.

While we do not calculate classical differential cross sections in this study, we develop a methodology that connects them to the collision cross sections through binning. Furthermore, we frequently utilize the one dimensional analogs of the classical differential cross section, which we call the vibrational/rotational differential cross sections. In the following section, we will describe these differential cross sections in more detail and explain how they are crucial to understanding the consequences of binning.

1.5 The Theory of Binning

Throughout the last two decades there have been several proposals which aim to assign the continuous classical distribution of rovibrational actions to discrete quantum numbers in a way that best encompasses quantum mechanical features [Stewart et al. [10], Bonnet and Rayez [11], Varandas [12], Bonnet and Espinosa-Garcia [13], Cotton and Miller [14]]. The growth of this field has been catalyzed by continued growth in

computing power. Many systems that were once inaccessible due to a lack of computational power, can now be simulated classically to a high degree of accuracy. As a result, new quasiclassical methods have emerged that make use of this abundance of data.

Before we discuss the latest developments in the field of binning, we clarify some of the terminology and mathematics that we will use. The binning function, denoted $W(|v_f - v_c|, |j_f - j_c|)$ describes a class of functions that exist at allowed rovibrational quantum numbers, which aid the assignment of trajectories to collision cross sections

$$\sigma(v_i, j_i \rightarrow v_f, j_f) = \pi b_{max}^2 \lim_{N\to\infty} \int\int \frac{\rho(v_c, j_c) W(|v_f - v_c|, |j_f - j_c|)}{N} dv_c \; dj_c. \quad (1.6)$$

As indicated by this equation, the weight that a trajectory is given toward the cross section at (v_f, j_f) is entirely dependent on the distances between its final classical action, (v_c, j_c) and the final quantum numbers, (v_f, j_f). We are able to describe the binning function in terms of these parameters because all of the binning functions that we utilize in this study are symmetric about the allowed quantum numbers [Bonnet and Rayez [11], Varandas [12], Cotton and Miller [14]]. As in previous approaches [Díaz et al. [5], Bonnet and Rayez [11]], we have chosen the binning functions to have a normalized area equal to the quantum number separation between allowed states,

$$W(|v_f - v_c|, |j_f - j_c|) = W_v(|v_f - v_c|) \; W_j(|j_f - j_c|), \quad (1.7)$$

$$\int W_j(|j_f - j_c|) \; dj_c = 2, \quad (1.8)$$

$$\int W_v(|v_f - v_c|) \; dv_c = 1. \quad (1.9)$$

Using Equations 1.5 and 1.6, we are able to express the cross section in terms of the classical differential cross section

$$\sigma(v_i, j_i \to v_f, j_f) = \int\int W(|v_f - v_c|, |j_f - j_c|) \frac{\partial^2 \sigma}{\partial v_c \partial j_c} dv_c \; dj_c. \tag{1.10}$$

As can be seen, the collision cross sections calculated using the binning function $W(|v_f - v_c|, |j_f - j_c|)$ are just the products of the classical differential cross sections and the binning functions, integrated over rovibrational phase space. Additionally, the magnitude of the calculated cross section as a function of binning method is entirely dependent on the overlap between the classical differential cross section and the binning function. Since the integral over the binning function is always normalized to the same value, it is only able to affect the calculation of the cross section by the way it weights the classical differential cross section.

Finally, we are also able to find an expression for the collision cross sections when one of the classical actions has been binned already. Integrating equation 1.6 over the variable j_c and remembering that the binning function is separable, we find that

$$\sigma(v_i, j_i \to v_f, j_f) = \int W(|v_f - v_c|) \frac{\partial \sigma}{\partial v_c} dv_c. \tag{1.11}$$

This quantity $\frac{\partial \sigma}{\partial v_c}$ will be referred to as the **vibrational differential cross section**. A similar equation can be derived by integrating over v_c, which expresses the cross section in terms of the **rotational differential cross section** $\frac{\partial \sigma}{\partial j_c}$

$$\sigma(v_i, j_i \to v_f, j_f) = \int W(|j_f - j_c|) \frac{\partial \sigma}{\partial j_c} dj_c. \tag{1.12}$$

We can use these expressions for the cross section to prove a lemma that we will find useful later. **When the vibrational/rotational differential cross section is linear with respect to the vibrational/rotational classical action, the collision cross section is independent of the vibrational/rotational binning function that is chosen.** While we will only prove this lemma for the rotational differential cross section, a very similar proof could be constructed for the vibrational differential cross section.

Since the binning function is symmetrical, a trajectory will be weighted equally if its rotational action deviates from the allowed quantum number by $+\Delta j_c$ or $-\Delta j_c$. As a result, if the derivative of the cross section is linear, the integral in Equation 1.12 will be independent of the choice of $W(|j_f - j_c|) = W(\Delta j_c)$. We define the variable "a" to describe the linearity of $\frac{\partial \sigma}{\partial j_c}$

$$\frac{\partial \sigma}{\partial j_c}|_{\Delta j_c} = (1 + a\Delta j_c)\frac{\partial \sigma}{\partial j_c}|_{j_f}. \tag{1.13}$$

We see that the integral in Equation 1.12 is independent of the weighting function by separating it into an integral over the states $\Delta j_c > 0$ and an integral over the states $\Delta j_c < 0$

$$\int_{-1}^{0} W(\Delta j_c)(1 + a\Delta j_c)\frac{\partial \sigma}{\partial j_c}|_{j_f} d\Delta j_c + \int_{0}^{1} W(\Delta j_c)(1 + a\Delta j_c)\frac{\partial \sigma}{\partial j_c}|_{j_f} d\Delta j_c. \tag{1.14}$$

The limits on the second integral can be reversed so that both integrals are over the trajectories with $\Delta j < 0$

$$\int_{-1}^{0} W(\Delta j_c)(1 + a\Delta j_c)\frac{\partial\sigma}{\partial j_c}|_{j_f} d\Delta j_c + \int_{-1}^{0} W(-\Delta j_c)(1 - a\Delta j_c)\frac{\partial\sigma}{\partial j_c}|_{j_f} d\Delta j_c. \quad (1.15)$$

Since the binning function is equal for Δj_c and $-\Delta j_c$, $W(\Delta j_c) = W(-\Delta j_c)$, the two integrals can be summed

$$2\int_{-1}^{0} W(\Delta j_c)\frac{\partial\sigma}{\partial j_c}|_{j_f} d\Delta j_c. \quad (1.16)$$

Since $\frac{\partial\sigma}{\partial j_c}|_{j_f}$ is a constant, and $W(\Delta j_c)$ is normalized, we can integrate over j_c to find

$$\sigma(v_i, j_i \to v_f, j_f) = 2\frac{\partial\sigma}{\partial j_c}|_{j_f}. \quad (1.17)$$

Noting that a similar argument will apply to the vibrational action we find

$$\sigma(v_i, j_i \to v_f, j_f) = \frac{\partial\sigma}{\partial v_c}|_{v_f}. \quad (1.18)$$

As we see, the collision cross-section is independent of binning function when the differential cross section is linear. Furthermore, we see that the value of the cross section is just the value of the differential cross section multiplied by a constant.

It is important to note that the value of the rotational differential cross section is dependent upon the way the vibrational action is binned, and vice versa. However, if one of the differential cross sections is always linear with respect to its action,

independent of how the other action is binned, this equality is very useful. In this situation, one is free to bin this classical action however one wishes.

Now that we have described some features of the binning function, we present an overview of some of the binning functions that have been used in the recent literature.

1.5.1 Standard Binning

The most frugal way to use trajectory data is to ensure that each trajectory is counted equally toward a particular collision cross section. In the past, the *de facto* method for accomplishing this was standard binning, which determines the final state of the classical trajectory by rounding the final vibrational [Gentry [6]] and rotational [Pattengill [15]] classical actions towards the nearest allowed quantum numbers. For our system, which is constrained by the selection rule that Δj must be even, the binning function can be expressed as

$$W(|v_f - v_c|, |j_f - j_c|) = \begin{cases} 1 & |v_f - v_c| < .5 \quad |j_f - j_c| < 1 \\ 0 & Otherwise \end{cases} . \tag{1.19}$$

While standard binning has largely fallen out of favor, it has two distinct advantages over binning methods that weight trajectories unevenly. Since every possible data point is used, standard binning has an excellent signal to noise ratio. The one sigma error bars on the standard binning cross section can be calculated as follows:

$$\delta\sigma_{v_f,j_f} = \frac{\sigma_{v_f,j_f}}{\sqrt{n_{v_f,j_f}}} \tag{1.20}$$

In the case that one of the differential cross sections is linear, standard binning can always be used to minimize computational work.

Additionally, since every trajectory is weighted by unity, **the standard binning cross sections are naturally normalized.**

$$\pi b_{max}^2 = \sigma_t = \sum_{\nu,j} \sigma_{\nu,j} \tag{1.21}$$

Unfortunately, standard binning's greatest asset, that it uses every trajectory, is also the source of its inaccuracies, since the final trajectories may gain or lose energy from the rounding of their final actions. As we will show, standard binning fails to produce accurate agreement with quantum mechanical results when the differential cross sections take on a shape that is neither linear nor sharply peaked. Additionally, standard binning fails to satisfy the classical condition of time reversal symmetry, microscopic reversibility, under similar circumstances.

1.5.2 Gaussian Binning

In 1997, Laurent Bonnet and J.C. Rayez proposed a solution to the rounding problem that had plagued standard binning. Instead of inaccurately assigning trajectories to quantum numbers that they do not represent, **gaussian binning only effectively utilizes trajectories whose final actions are very close to allowed quantum numbers** [Bonnet and Rayez [11]]. Gaussian binning relies on the assumption that the best classical analog of a quantum transition is a classical trajectory that begins at the initial quantum number and ends at the final quantum number. Using this

framework, a rejection of the trajectories that do not land at allowed final quantum numbers is a type 1 error, as trajectories that do not satisfy $\Delta v, \frac{\Delta j}{2} \in \mathbb{Z}$ could still represent true rovibrational transitions. However, if these trajectories do not accurately represent rovibrational transitions, counting them runs the risk of the far more harmful type 2 error [Bonnet and Rayez [11]]. In 2004 Bonnet and Rayez further justified this procedure through classical S-Matrix theory [Bonnet and Rayez [16]].

In its ideal implementation, gaussian binning would only utilize trajectories that land at allowed quantum numbers, which would amount to using delta-functions as the binning functions. However, since no trajectories land exactly on the final quantum number in practice, gaussian binning must make approximations. Bonnet and Rayez approximate the delta-functions with narrow-width gaussians centered at the allowed quantum numbers, typically with a full-width at half maximum (FWHM) that is 10% of the quantum number separation. This ensures that only trajectories whose final actions are very close to allowed final quantum numbers are able to contribute significantly to the cross sections.

Unfortunately for our study, Bonnet and Rayez do not outline a method for binning in rotational space, where selection rules outlaw certain states. In order to generalize their work, we bin our rotational states using a gaussian with a full-width at half maximum equal to 10% of the distance between allowed quantum numbers, or 10% of a standard bin width. Since only transitions that satisfy Δj even are allowed for Li_2, we use a rotational gaussian that is twice the width of the vibrational gaussian. The gaussian curves are normalized according to Equations 1.8 and 1.9. The weight

of each trajectory towards the collision cross section (v_f, j_f) using gaussian binning, is calculated for our system as follows

$$W(|v_f - v_c|, |j_f - j_c|) = \frac{1}{2\pi\sigma^2} exp(-\frac{(v_c - v_f)^2 + ((j_c - j_f)/2)^2}{2\sigma^2}). \tag{1.22}$$

where v_f and j_f are the closest allowed quantum numbers. σ is the standard deviation, related to the full-width at half maximum (FWHM) by the following relation

$$FWHM = 2\sqrt{2\ln 2}\sigma \approx 2.355\sigma. \tag{1.23}$$

Unless otherwise specified, the FWHM is set to equal 10% of the standard bin width, the value that has been most frequently used in the literature [Banares et al. [1], Balucani et al. [2, 3], Czakó and Bowman [4]]. We find that the cross section calculated with a FWHM of 10% is in relatively good agreement with the predicted value of the cross section as FWHM $\rightarrow$ 0. When the dependence of the cross section on the FWHM is fit with a power law function, the extrapolated behavior is close to the value at FWHM = .1 (Figure 1.1).

While we see good convergence at 10%, other studies have suggested that an even narrow width gaussian may be required in certain cases [Carmona-Novillo et al. [17]].

As said earlier, the major advantage of gaussian binning is that it effectively deals with the quantization problem, as it only utilizes data that accurately reflects the true classical version of the quantum number transitions. Through only utilizing these 'allowed' trajectories, **gaussian binning has been shown to predict the rovibrational state distributions of a wide variety of reactive collisions**

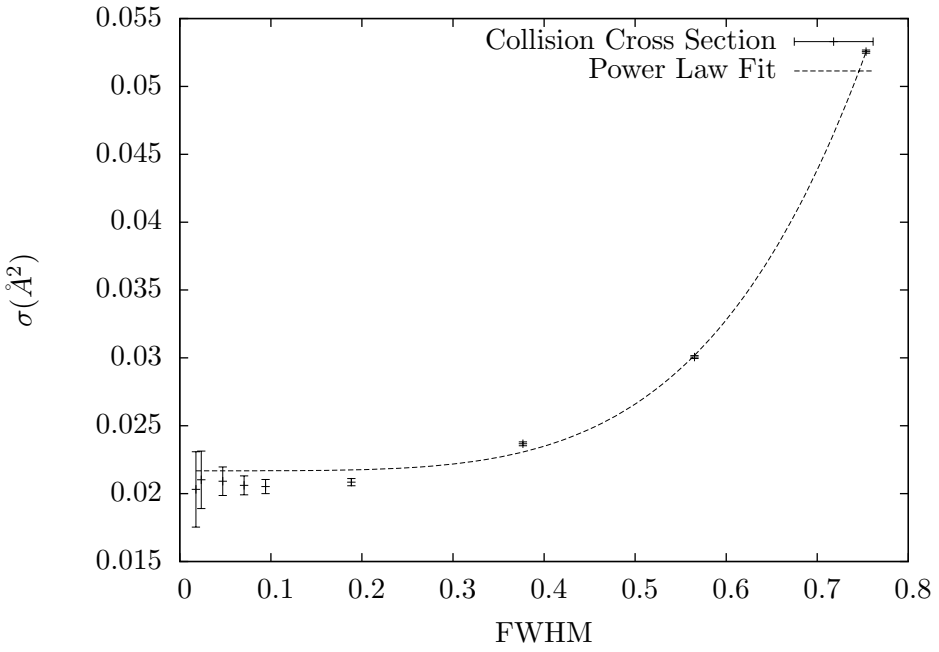

FIGURE 1.1: Collision cross sections calculated using gaussian binning plotted as a function of FWHM for $(v_i = 0, j_i = 18) \rightarrow (v_i = 1, j_f = 38)$. The data is fit with a power law function that models the behavior of the cross section as FWHM $\rightarrow 0$

better than standard binning [Balucani et al. [3], Banares et al. [18], Xie et al. [19]]. Specifically, gaussian binning has been shown to correct cross section distributions that end up shifted towards rotationally excited states due to trajectories being assigned extra vibrational energy during the standard binning process [Banares et al. [1], Jorfi et al. [20]]. In Chapter 3, we will show that gaussian binning improves agreement in the Li_2 + Ne system, but in a different way than others have seen.

However, we will see that despite improving agreement with quantum mechanics in most places, gaussian binning can cause statistical issues that render it worthless in certain situations. Unlike the standard binning cross sections, the gaussian binning cross sections are not naturally normalized, as trajectories can be weighted by much

more than or less than one on average. For example, if the trajectories land disproportionately near the allowed quantum numbers where they are weighted heavily, the cross sections may become unrealistically large. Conversely if the trajectories disproportionately land far away from the peaks of the binning functions, the cross sections may become very small. If the final cross sections are renormalized to sum to πb_{max}^2, a grossly overestimated cross section could seriously affect the value of the other cross sections. Bonnet and Rayaz proposed that in order to alleviate this issue, one should always choose the smaller cross section between the standard binning and gaussian binning results. The cross sections could then be normalized using the following equation

$$\sigma_{v_f,j_f} = \pi b_{max}^2 \frac{\sigma_{v_f,j_f}^{-}}{\sigma_t}, \tag{1.24}$$

where σ_{v_f,j_f}^{-} is the smaller cross section between standard and gaussian binning.

Although this methodology is able to fix the major computational problems associated with gaussian binning, it fails to account for the case in which the gaussian binning cross section is both larger and more accurate than the standard binning cross section. In Chapter 5, we will give an example of such a case, and attempt to establish a better condition for choosing between the standard and gaussian binning cross sections.

Another drawback to gaussian binning is the inherent data loss. Since the FWHM parameter is usually set to be 10% of a bin width, gaussian binning utilizes an order of magnitude less data for each degree of freedom. While Bonnet has provided a good

way to mitigate this data loss in systems with many vibrational modes [Bonnet and Espinosa-Garcia [13]], there has been no effective way to treat this in rovibrational gaussian binning, which reduces signal to noise by two orders of magnitude. We find that even 10^8 trajectories are sometimes unable to produce usable data for gaussian binning.

Finally, before we discuss other methods that attempt to treat this quantization problem, we consider the limiting case of a gaussian binning function with a FWHM of zero. In this limiting behavior, the gaussian function becomes a delta-function

$$\sigma_{db}(v_i, j_i \rightarrow v_f, j_f) = \pi b_{max}^2 \lim_{N\rightarrow\infty} \int\int \frac{n(v_c, j_c)\delta(v_f - v_c)\delta(j_f - j_c))}{N} dv_c \; dj_c. \quad (1.25)$$

When we evaluate this integral, noting that the number of trajectories at $n(v_c, j_c)|_{v_f,j_f}$ is equivalent to $\rho(v_c, j_c)|_{v_f,j_f}$ we can solve for the delta-function binning cross section in terms of the classical differential cross section. Noting that the integral over a (dv_c, dj_c) standard bin is equal to two, we find that

$$\sigma_{db}(v_i, j_i \rightarrow v_f, j_f) = 2\frac{\partial^2\sigma}{\partial v \partial j}|_{v_f,j_f}. \quad (1.26)$$

We have shown that the delta-function binning cross section can be calculated by doubling the value of the classical differential cross section evaluated at the final quantum number. As a result, the classical cross section is an excellent tool for doing narrow-width binning, as it not only provides information about the narrow-width cross section itself, but it provides data points in the immediate vicinity.

Finally, it can be shown that when the vibrational/rotational action is already

binned, and delta-functioned binning is done on the rotational/vibrational action, the value of the cross section can be expressed as a function of the rotational/vibrational differential cross section using the following relations

$$\sigma_{db}(v_i, j_i \rightarrow v_f, j_f) = 2\frac{d\sigma}{dj_c}|_{j_f} = \frac{d\sigma}{dv_c}|_{v_f}. \tag{1.27}$$

As a result, the vibrational and rotational differential cross sections can be utilized to bin with a narrow width in one dimension. In Chapter 3, we will utilize this trick to improve the agreement between the QCT calculations and quantum mechanics for vibrationally elastic collisions.

Although this study will only use gaussian binning and other narrow-width methods to study quantization problems, we present a brief overview of other proposals that address similar issues.

1.5.3 Momentum Gaussian Binning and other Zero-Point Leakage Methods

Although the gaussian function is synonymous with quantum uncertainty, Bonnet and Rayez [Bonnet and Rayez [11, 16]] ultimately choose it for statistical reasons in the gaussian binning producedure, not physical ones. In our data we find that the gaussian function provides an ideal shape for narrow-width binning, as the tails play a strong role in stabilizing the error. We find that gaussian binning produces a better signal to noise ratio than a similar 'fractional binning' approach, which heavily

weights trajectories inside the range of the gaussian FWHM and ignores trajectories outside of it

However, A.C. Varandas recently suggested that gaussian binning should be done in a way that is compatible with quantum uncertainty [Varandas [12]]. Varandas models the collision as a Gaussian Wave-Packet, which maintains a gaussian position-momentum uncertainty that spreads during time evolution. He argues that the binning should be done in a way that preserves the momentum uncertainty of quantum mechanics. Since the vibrational momentum, $p_v \propto \sqrt{(}E_v) \propto \sqrt{(}v_f)$, and the rotational momentum $p_j \propto \sqrt{(}E_v) \propto j$, the trajectories should be binned as follows

$$W_{|v_f - v_c|,|j_f - j_c|} \propto exp(-\frac{(\sqrt{(}v_c) - \sqrt{(}v_f))^2}{\alpha\ \sqrt{(}v_f)} - \frac{(j_c - j_f)^2}{\beta\ j_f}), \tag{1.28}$$

where α and β are parameters that describe the spreading of the wave packet. Unfortunately, to determine this spreading would require a quantum mechanical calculation. As a result, the width parameters α and β cannot be determined using classical methods. However, Varandas conjectures that the ratio in the spread of the momentum distributions of different degrees of freedom should be roughly inversely proportional to the ratio of the energy level separations. For Li_2 this condition manifests itself in this form.

$$\frac{\beta}{\alpha} = \frac{519}{j} \tag{1.29}$$

In order to determine the absolute magnitude of the spreading parameters, Varandas used his physical intuition, noting that choosing $\alpha = .1$ allowed trajectories with

a $v_c = .9$, to be given 48% of the weight of trajectories with $v_c = 1$ towards the final cross-section. However, in our system such a choice would lead to a rotational spreading parameter of $\beta = \frac{51.9}{j}$, leading to extremely wide rotational gaussians, especially around $j = 0$. This choice of parameter would most likely lead to significant averaging over the rotational cross sections. As a result we do not believe this method is useful for the Li_2 system, or any system with a significant disparity between the vibrational and rotational energy level spacings. Since gaussian binning also provides a solution for the zero-point leakage problem [Jorfi et al. [20], Zhang et al. [21]], and has been more tested more thoroughly, we choose to focus our study on gaussian binning.

Finally, we briefly mention methods that have been used to confront zero-point leakage in the past, but are less useful due to improvements in computational power [Kumar et al. [22]]. A method pioneered by Mandy and Martin [Mandy and Martin [23]], involves calculating the cross sections of the reverse processes, which do not exhibit zero-point leakage, then using the equation of microscopic reversibility to calculate the forwards cross sections. This was shown to give far better results than standard binning for the H + H_2 reaction.

In the past, our laboratory would confront zero-point leakage by choosing the final rotational action in order to minimize the energy difference between the final classical rovibrational state and the binned rovibrational state. This method of 'energy rounding' is useful when the extra vibrational zero-point energy leaks into the rotational degrees of freedom, as this method will compensate for the added vibrational energy by subtracting rotational energy. However, when the zero-point energy leaks

into translational energy instead, this method will artificially shift the rotational distribution.

Finally, another common solution involved completely ignoring trajectories that did not end up with their full vibrational zero-point energy [Varandas [24]]. Although all of these methods have been shown to reduce zero-point leakage, we choose to use gaussian binning because of its prolific recent success.

1.5.4 Symmetrical Windowing

While the binning methods described in the previous sections limit their scope to the quantization and zero-point issues issues that arise in the QCT, the method of symmetrical windowing [Cotton and Miller [14]] attempts to incorporate wave effects. Specifically it aims to account for the threshold smoothing that occurs due to quantum tunneling. In this method, proposed by Steven Cotton and William Miller, both the initial and final quantum numbers are treated as a distribution of classical actions. First a windowing function is chosen, which can either be a histogram or a gaussian. Instead of starting the trajectories at the initial quantum number, as is done in other methods, the initial actions are chosen to form a distribution that takes the shape of the windowing function. The equations of motion are then solved using this initial distribution of classical actions, and the trajectories are binned over an function that is identical to the one they were sampled over. For our system,

gaussian symmetrical windowing should be done as follows

$$P(|v_f - v_c|, |j_f - j_c|) = W(|v_f - v_c|, |j_f - j_c|), \tag{1.30}$$

$$W(|v_f - v_c|, |j_f - j_c|) = \frac{1}{sqrt(2\pi\sigma)} exp(-\frac{(v_f - v_c)^2 + (j_f - j_c)^2}{2\sigma^2}), \tag{1.31}$$

where $P(|v_i - v_c|, |j_i - j_c|)$ represents the probability of sampling a trajectory around initial quantum number (v_i, j_i), and $W(|v_f - v_c|, |j_f - j_c|)$ represents the weight of a trajectory towards the cross section at v_f, j_f with the final action v_c, j_c. Similarly, the histogram version of this approach would sample and bin in a symmetrical fashion

$$W(|v_f - v_c|, |j_f - j_c|) = \begin{cases} 1 & |v_f - v_c| < \frac{WIDTH}{2} \quad |j_f - j_c| < WIDTH \\ 0 & Otherwise \end{cases}. \tag{1.32}$$

Cotton and Miller found that in determining the reaction probability of collinear H + H_2 scattering, optimal agreement with quantum mechanical results was obtained at an effective windowing width (FWHM, WIDTH) of half a standard bin. Additionally, they found that the effective width of the windowing function was much more important than the shape of the distribution that was used.

They believed that this improved agreement was due to trajectories whose initial vibrational actions were sampled towards higher v_c, and therefore able to cross the reaction threshold more easily. This effect should be most prominent very close to the threshold, where this kind of sampling may give some trajectories the extra energy they need to be boosted over the threshold. At higher energies, this effect should wash out, as an equal number of trajectories will lose energy through sampling as

will gain energy. Taking these qualitative ideas into account, this effect should result in a smoothing of the threshold.

As we will show later, we also see strong disagreement between the QCT and quantum mechanics near the vibrational excitation threshold in the Li_2 + Ne system. While quantum mechanics predicts that vibrational transitions should be possible down to an energy 380 cm^{-1}, the QCT begins to predict vibrational transitions around 1250 cm^{-1}. In the hope that we may be able to improve upon the threshold problem, we study the effect of symmetrical windowing on the energy dependence of the cross-section.

1.6 Approach of this Study

We begin our study by describing the important features of the Li_2 + Ne system in Chapter 2. In Chapters 3-5 we test the different binning methods with two criteria in mind: Do these results produce good agreement with quantum mechanics? Are these methods done in a classically and statistically correct manner? The fulfillment of both criteria is essential to claiming that a method can produce a physically accurate, generalizable model.

1.6.1 Agreement with Quantum Mechanical Results

In order to evaluate our quasiclassical trajectory methods, we compare them to the quantum mechanical results obtained in a previous study in our lab [Stewart et al. [25]]. These results calculate the quantum mechanical cross sections using an

implementation of the MOLSCAT program [Hutson and Green [26], McBane and Valiron [27]], that utilizes the same Alexander and Verner potential energy surface [Alexander et al. [9]].

We primarily evaluate the empirical agreement between our binning methods and quantum mechanics in two ways. In Chapter 3, we look for agreement at the energy, $E = 2500$ cm^{-1}, as this is an energy where quantum mechanics and classical mechanics should begin to converge. However, as we will show, there is still significant disagreement between the QCT and quantum mechanics at this energy, especially for vibrationally inelastic collisions. We show that judicious use of a narrow-width binning method like gaussian binning is able to noticeably improve upon this agreement .

We then move toward the threshold energies, where classical mechanics and quantum mechanics diverge much more strongly. In Chapter 4, we show that the classical and quantum cross sections agree very poorly for most final rovibrational quantum numbers at low energy. Additionally, we show that the symmetrical windowing method, which was shown to result in threshold smoothing in the one dimensional $H + H_2$ system, is only mildly effective at smoothing the threshold in the $Li_2 + Ne$ system.

After we study the empirical agreement between classical and quantum mechanics in Chapters 3-4, we test the QCT methods for time reversal symmetry in Chapter 5.

1.6.2 Microscopic Reversibility

In order to test our binning methods for time-reversal symmetry, we examine a property called microscopic reversibility, which arises from the fact that Newton's equations are time-invertible. Within classical mechanics, for every trajectory traveling from (v_i, j_i) to (v_f, j_f), there exists a reverse trajectory with an opposite velocity that travels from (v_f, j_f) to (v_i, j_i). **Microscopic reversibility states that as a consequence, in equilibrium, the rate of a forward process is equivalent to the rate of the backwards process** [Tolman [28]]. Through this rate equality, we can derive an equation that relates the cross sections of the forward and reverse processes [Polanyi and Schreiber [29]]

$$\sigma_{v_i,j_i \to v_f,j_f}(E_t - E_{v_i,j_i})(2j_i + 1), = \sigma_{v_f,j_f \to v_i,j_i}(E_t - E_{v_f,j_f})(2j_f + 1), \tag{1.33}$$

where $E_{v,j}$ represent the internal energy of the diatom in the $(v,\ j)$ state, E_t represents the total energy, and $(v_i,\ j_i)$, $(v_f,\ j_f)$ represent rovibrational states. This study tests whether a procedure is microscopically reversible, by examining how close the following quotient is to one

$$MRC = \frac{\sigma_{v_i,j_i \to v_f,j_f}(E_t - E_{v_i,j_i})(2j_i + 1)}{\sigma_{v_f,j_f \to v_i,j_i}(E_t - E_{v_f,j_f})(2j_f + 1)}. \tag{1.34}$$

When we began this study, we believed that the binning function would play a strong role in determining whether a process will be microscopically reversible. We hypothesized that the condition for microscopic reversibility is a resemblance between the shape of the sampling curve and the product of the binning function with

the classical differential cross section. We attempt to justify this in the following few paragraphs.

During the sampling process, the initial quantum number is set to equal a distribution of classical actions. Since every trajectory contributes to a cross section that begins at the initial quantum number, the integral over the classical representations of the initial state should equal to one

$$\int\int P(v_c, j_c) dv_c dj_c = 1, \tag{1.35}$$

where $P(v_c, j_c)$ is just the probability of choosing a particular initial classical action. In order to come up with a condition for microscopic reversibility, we would like to find the quantity that corresponds to the final quantum number in the same way that the initial distribution of classical actions corresponds to the initial quantum number. We argue that the integral over the classical representations of the final state should be equal to the effective proportion of trajectories that contribute to the final state. We are able calculate this proportion from the collision cross section

$$\frac{n_{v_f,j_f}}{N} = \frac{\sigma_{v_f,j_f}}{\pi\ b_{max}^2}. \tag{1.36}$$

Using this relation and Equation 1.10 for the collision cross section, we find that

$$\frac{n_{v_f,j_f}}{N} = \frac{1}{\pi b_{max}^2} \int\int \frac{\partial^2 \sigma}{\partial v_c\ \partial j_c} W(|v_f - v_c|, |j_f - j_c|) dv_c dj_c. \tag{1.37}$$

This quantity that is integrated over, $\frac{1}{\pi b_{max}^2} \frac{\partial^2 \sigma}{\partial v_c\ \partial j_c} W(|v_f - v_c|, |j_f - j_c|)$, is related to the final quantum number in the same way that $P(|v_f - v_c|, |j_f - j_c|)$ is related

to the initial quantum number. In order for time-reversal symmetry to hold, these two distributions should be identical. The reverse trajectory should be represented by the same distribution of actions when it is sampled at (v_f, j_f) that represents the forwards trajectory when it is binned to (v_f, j_f). Additionally, the distributions must agree similarly around the initial quantum number. **The condition for time-reversal symmetry in the quasiclassical trajectory method is**

$$\frac{1}{\pi b_{max}^2}\frac{\partial^2\sigma}{\partial v_c\,\partial j_c}\,W(|v_f - v_c|, |j_f - j_c|) = P(|v_f - v_c|, |j_f - j_c|), \tag{1.38}$$

for all (v_c, j_c) and (v_f, j_f). We can also separate this equation into two separate conditions for rotation and vibration

$$\frac{1}{\pi b_{max}^2}\frac{\partial\sigma}{\partial v_c}\,W_v(|v_f - v_c|) = P_v(|v_f - v_c|), \tag{1.39}$$

$$\frac{1}{\pi b_{max}^2}\frac{\partial\sigma}{\partial j_c}\,W_j(|j_f - j_c|) = P_j(|j_f - j_c|). \tag{1.40}$$

In Chapter 5, we show that gaussian binning satisfies microscopic reversibility well, as the narrow width binning function eliminates most of the asymmetry in the classical differential cross sections. Since the initial trajectories are effectively sampled using delta-functions, both the classical representation of the initial quantum number $P(|v_f - v_c|, |j_f - j_c|)$, and the classical representation of the final quantum number $\frac{1}{\pi b_{max}^2}\frac{\partial^2\sigma}{\partial v_c\,\partial j_c}\,W(|v_f - v_c|, |j_f - j_c|)$ are narrowly peaked if $W(|v_f - v_c|, |j_f - j_c|)$ is narrowly peaked. We also show that standard binning fails to satisfy microscopic reversibility when the final distribution of classical actions is non-linear, as the uniform weighting allows the classical representation of the final quantum number to

maintain its non-linear shape. Finally, we show that symmetrical windowing is also not microscopically reversible in our system for similar reasons.

We now move on to Chapter 2, where we will discuss $Li_2 + Ne$ in detail.

Chapter 2

Features of the Li_2 + Ne Collision System

In this chapter we will give a brief overview of the Li_2 + Ne collision system by discussing interesting features of the classical simulation, and showing how its predictions diverge from those of quantum mechanics. While classical mechanics describes the Li_2 + Ne system adequately in certain areas, it is very inaccurate in others. In order to search for the source of the disagreement, we examine the magnitude of quantum effects that are not included in the classical simulation.

2.1 Wave Effects

The de Broglie wavelength of the entire system, which roughly gauges the magnitude of wave effects, can be expressed as a function of the relative velocity between the

atom and the diatom. For the $Li_2 + Ne$ system

$$\lambda(\text{Å}) = \frac{\hbar}{\mu v_{rel}} = \frac{7.68 * 10^{-2}}{v_{rel}(\text{km/s})}. \tag{2.1}$$

Over the velocity range in which vibrationally inelastic scattering is possible according to classical mechanics, $v_{rel} > 1$ km/s, the de Broglie wavelength does not exceed 7.68 pm. Given that the internuclear separation of Li_2(A) is approximately 311 pm, the length scale of the de Broglie wavelength is at least an order of magnitude less than the length scale of the collision. As a result, **we do not expect wave effects to play a significant role in the collision dynamics**. Furthermore, because the collision cross section is averaged over a wide variety of orientations, we should expect wave effects to average out to a large degree [Pattengill [15], Bonnet [30]].

2.2 Quantization Effects

While we do not expect interference to affect our cross sections significantly, we do believe that quantization effects, which emerge because classical mechanics does not discretize bound states, significantly affect the collision cross sections. While the rotational energy levels of the Li_2 + Ne system at 2500 cm^{-1} are relatively close together within the accessible range of classical phase space, the vibrational levels are spread out much more. In the approximation that the rotational and vibrational degrees of freedom are separable within the molecule, the rigid rotor

harmonic oscillator approximation can be used.

$$E_{rot} = B_e j(j+1) \tag{2.2}$$

$$E_{vib} = \omega_e(v + \frac{1}{2}) \tag{2.3}$$

Under this approximation, the spacing between vibrational levels is ω_e. Since Li_2 is homonuclear and has D_∞ symmetry about its center of mass, selection rules dictate that only transitions of even Δj can occur. As a result, the spacing between allowed rotational levels for a given process is $B_e[(j+1)(j+2) - (j-1)j] \approx 4B_e j)$. For Li_2, $B_e = .492$ cm^{-1} and $\omega = 255.47$ cm^{-1}. The energy level spacing is as follows:

$$\Delta E_{rot} = 1.968j \text{ cm}^{-1} \tag{2.4}$$

$$\Delta E_{vib} = 255.47 \text{ cm}^{-1} \tag{2.5}$$

While the vibrational energy level spacing is more than 10% of the available collision energy, the rotational energy level spacing is under 2% of the available collision energy at $j_f = 18$. Unsurprisingly, **the vibrational differential cross section has significant non-linear features on the length scale of its quantum number separation**. (Figure 2.1). **On the other hand, the rotational differential cross section is usually roughly linear on the length scale of its allowed quantum number separation** (Figure 2.2).

As we showed on Page 19-20 of the introduction, a calculation of the collision cross will be independent of binning method when the differential cross section is linear. As a result, we do not expect the binning of the rotational action to have a significant

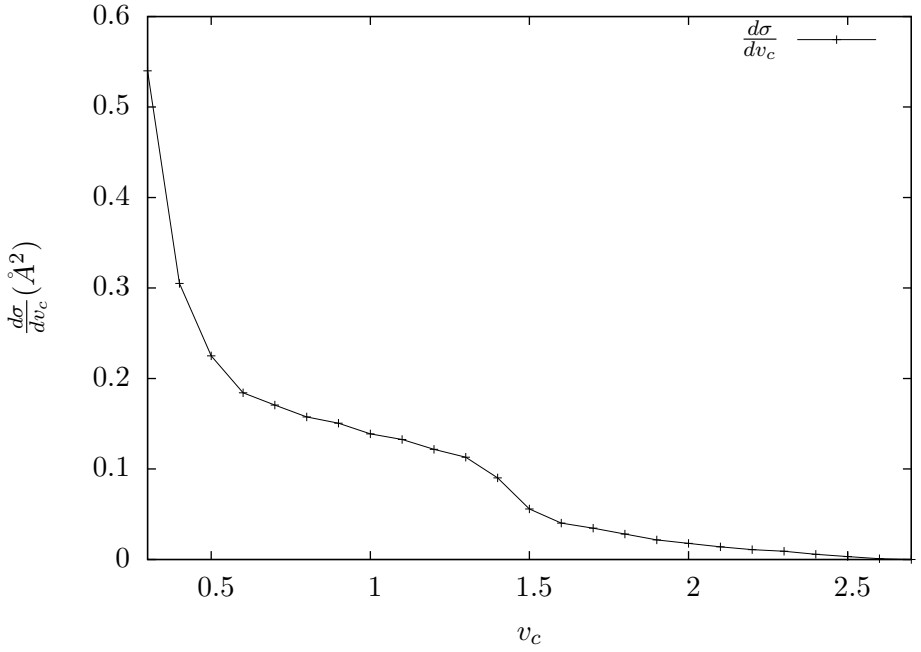

FIGURE 2.1: Vibrational differential cross section for the process $(v_i = 0, j_i = 18) \rightarrow j_f = 18$. The vibrational differential cross section curves significantly over the range of a quantum number.

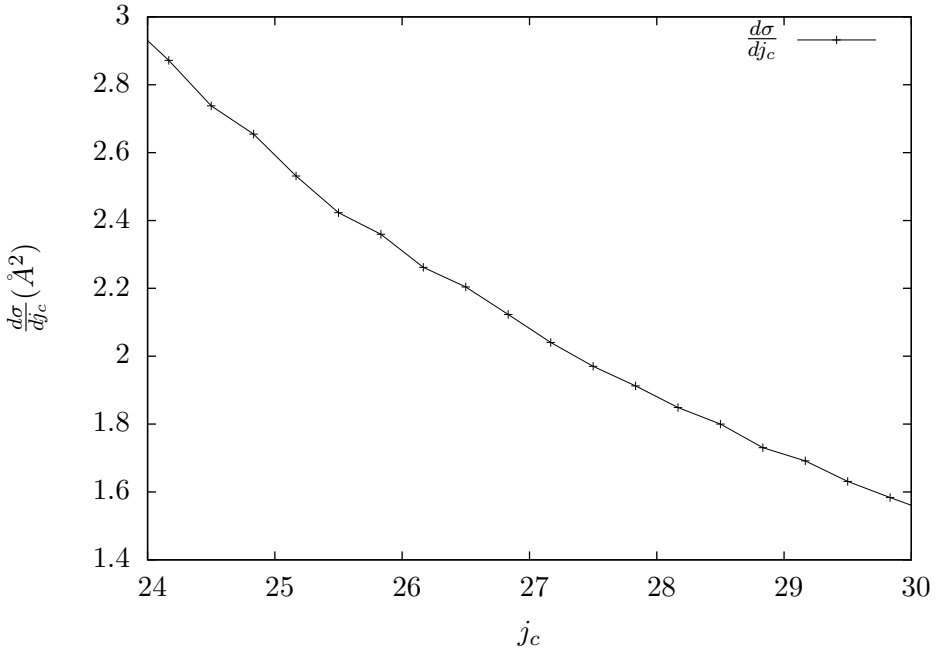

FIGURE 2.2: Rotational differential cross section for the process $(v_i = 0), j_i = 18 \rightarrow v_f = 0$ plotted over three allowed rotational states. The rotational differential cross section does not curve significantly over the range of a quantum number.

effect on the collision cross section. From this we conjecture that quantization effects will be unimportant in rotation at 2500 cm^{-1}. However, since the vibrational actions are highly non-linear on the scale of a quantum number, we expect that quantization of the final vibrational action will play a serious role in agreement with quantum mechanics.

For vibrationally inelastic collisions at 2500 cm^{-1}, the QCT with standard binning disagrees moderately with quantum mechanics. (Figure 2.3). While the QCT with

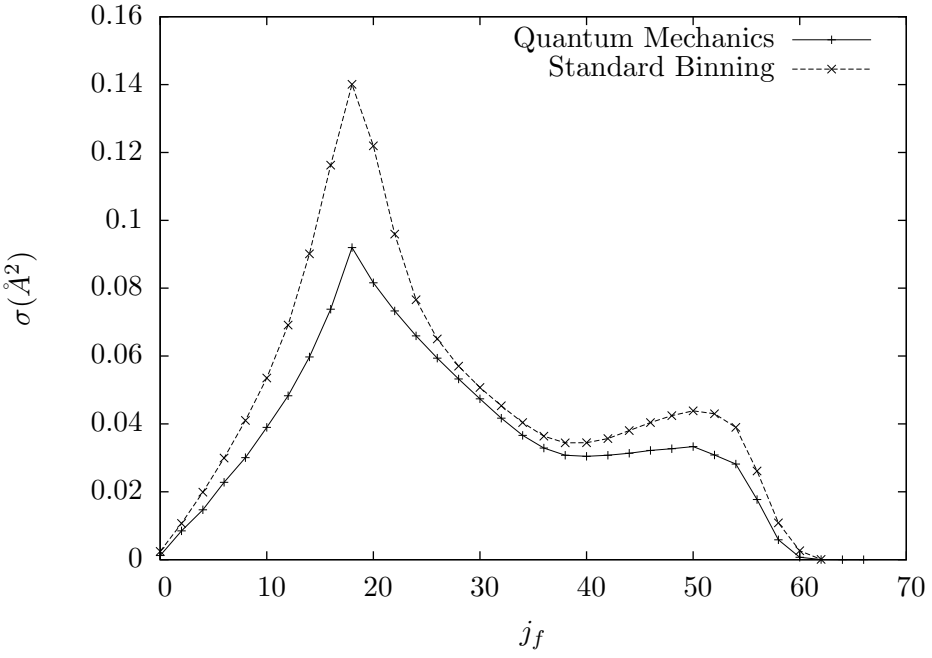

FIGURE 2.3: Vibrationally inelastic cross sections as a function of final rotational quantum number using quantum mechanics and the QCT with standard binning

standard binning predicts a larger peak at $j_f = 18$, it does a good job of predicting the qualitative shape of the rotational distribution. We hypothesize that this disagreement occurs due to an incorrect quantization of the classical vibrational actions, which we will investigate in the following chapter. We will show that quantizing the final classical actions using a narrow-width binning method is able to

improve agreement with quantum mechanics in some situations.

2.3 Other Quantum Effects

While we do not expect wave effects to be significant at any energy, we see that non-quantization quantum effects are significant at lower energies. While the classical threshold for vibrational excitation cuts off at a value of ≈ 1300 cm^{-1}, the quantum mechanical threshold gently declines until 380 cm^{-1} (Figure 2.4). In Chapter

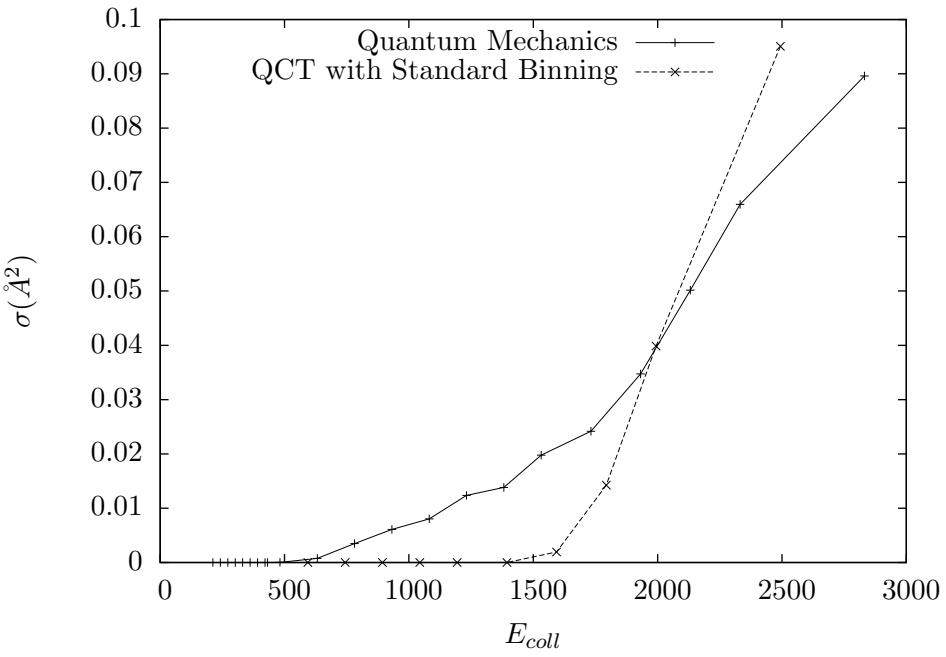

FIGURE 2.4: Collision cross sections as a function of collision energy for the $(v_i = 0, j_i = 18) \rightarrow (v_f = 1, j_f = 24)$ transition using quantum mechanics and the QCT with standard binning

4, we will attempt to improve upon this agreement by implementing the symmetrical windowing method in the hopes that it will allow more trajectories to undergo vibrational excitation at low energies.

However, before we add additional quantum effects to our study, we examine quantization effects in isolation, through choosing an energy of 2500 cm^{-1}, where we expect other quantum effects to be small. We now move on to Chapter 3, where we look at the agreement between the QCT and quantum mechanics in the high energy regime.

Chapter 3

Agreement with Quantum Mechanical Results at High Energy

3.1 Introduction

Now that we have introduced binning and given a brief overview of our collision system, we study the empirical agreement between different implementations of the QCT and quantum mechanics. We begin by studying the behavior of our system at a total energy of 2500 cm^{-1}. We choose this energy because we believe that all of the quantum effects will be small besides the discretization of bound states. In the $(v_i = 0,\ j_i = 18)$ state of Li_2, with a total energy of 2500 cm^{-1} the relative velocity of the atom with respect to the diatom is $v_{rel} = 269,137$ cm/s. At this collisional

velocity, the de Broglie wavelength is small relative to the length scale of the collision

$$\lambda = 2.85pm \approx .012 * r_{eq}(Li_2). \tag{3.1}$$

As a result, we expect that wave effects should be very small, and most of the disagreement between classical and quantum mechanics should lie in quantization effects.

3.2 Zero Point Leakage

This study focuses on collision cross sections from the initial rovibrational state, $(v_i = 0,\ j_i = 18)$. **States in which the initial diatom is not vibrating are particularly interesting because the treatment of the vibrational zero point energy is especially consequential.** The zero point energy in our system is reflected in the fact that trajectories acquire vibrational actions as low as $v = -1/2$ during the course of the collision. However, unlike in quantum mechanics, there is no classical constraint that forces the molecule to regain its zero point energy at the end of the trajectory. As a result, the original vibrational zero point energies of the classical trajectories can end up in other degrees of freedom at the end of the collision. Using standard binning, these trajectories will be treated as contributors to the $v_f = 0$ cross section, and therefore will be reassigned the energy that they had lost. As a result, the binned trajectory will have extra energy in its other degrees of freedom despite having the same vibrational energy.

A similar problem occurs when a trajectory ends up with a final vibrational action satisfying $.5 < v_c < 1$. Using standard binning, these trajectories are assigned to the $v_f = 1$ cross section. As a result, the final classical states can be thought of as $v_f = 1$ states without their zero point energy. Again, this extra energy, which is the difference between the energy of the classical and the quantum state, can become part of a different degree of freedom. When trajectories are consistently assigned energy through rounding, other degrees of freedom can become hotter than they should be. It has been shown in many cases that zero point leakage may lead to rotationally hot distributions, [Xie et al. [19], Jorfi et al. [20]].

In order to gauge the potential magnitude of this effect on our system, consider a Li_2 molecule that begins in the state $v = 0$ with a zero-point vibrational energy of 128 cm^{-1}. If this molecule's vibrational action decreases from $v = 0$ to $v = -.5$, it could gain enough rotational energy to transition from $j = 18$ to $j = 24$. Using standard binning, this trajectory would be counted towards the $v = 0$ vibrational state, **and rotational energy will have emerged from nothing**. If this effect were to occur consistently, the distribution of rotational quantum states could be skewed towards the high j_f range.

If the vibrational zero-point energy were to exclusively leak into rotation, the issue could adequately be treated with the energy-based rounding techniques discussed in the previous chapter. In this method, the final rovibrational actions are reassigned so that the internal energies of the final classical state and the assigned quantum state are equal. Therefore, when a trajectory with a negative final vibrational action

gains internal energy through being assigned to the $v_f = 0$ state, it will be stripped of the equivalent amount of rotational energy before it is binned.

However, in cases in which the vibrational zero-point energy leaks into the energy of the scattered atom, it does not make physical sense to compensate by subtracting rotational energy. Gaussian binning, which simply ignores the bad data instead of making corrections for it, provides a more physically accurate way to avoid zero point leakage. However, as we will see gaussian binning engenders its own serious issues. The non-vibrating state, ($v_i = 0,\ j_i = 18$), provides a good place to begin investigating these phenomena.

3.3 Vibrationally Elastic Collisions

We begin by studying vibrationally elastic collisions at 2500 cm^{-1}, where the collision cross sections should agree well with quantum mechanics. At this collision energy, the available energy and momentum far exceed the threshold for rotational excitation. However, we still could be confronted by the vibrationally elastic zero point leakage problem described in the previous section. Luckily, this does not occur in our system because the final distribution of final vibrational actions is very dense and symmetric about the point $v_c = 0$ (Figure 3.1). The very dense line of trajectories at the center indicates that most trajectories are almost completely classically vibrationally elastic, even when they undergo a significant change in rotational state. Additionally, due to the symmetry about the $v_c = 0$ point, an equal number of trajectories would lose energy from standard binning as would gain energy. As a result, we do not

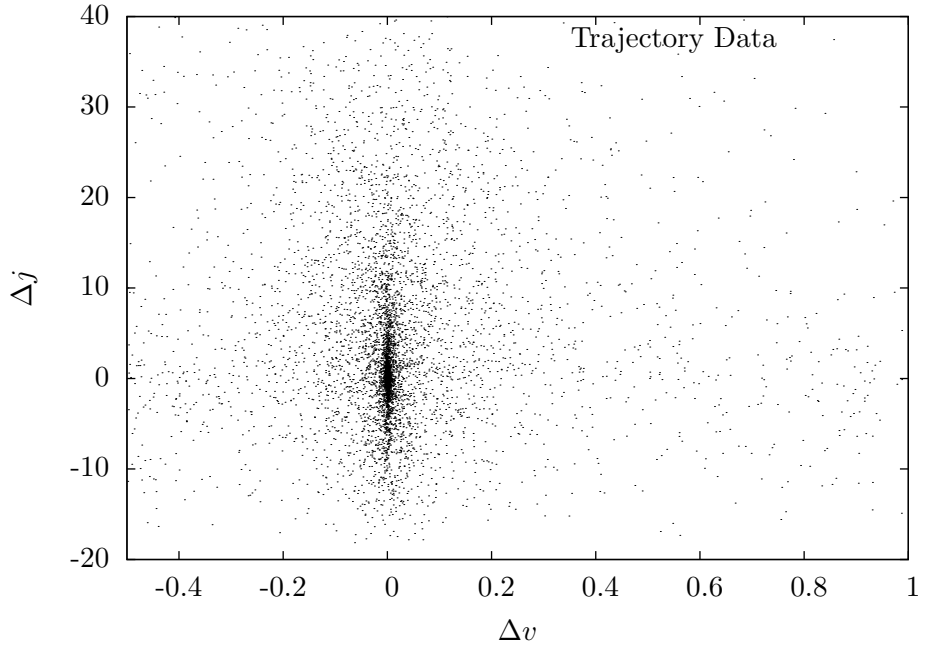

FIGURE 3.1: Change in the rotational action plotted against the change in vibrational action for 10,000 trajectories at 2500 cm^{-1}

expect the standard binning distribution of rotational states to be shifted due to zero point energy leakage.

Indeed, the standard binning cross sections agree relatively well with the quantum calculations in both magnitude and shape (Figure 3.2). The two distributions are shaped very similarly, and agree very well in magnitude except at $\Delta j = \pm 2$, where standard binning overestimates the collision cross section by about 25%. Interestingly, standard binning provides its largest overestimate in the area where the rotational differential cross section is most highly curved (Figure 3.3)

As a result of this finding, we suspect that standard binning overestimates the collision cross section due to the non-linearity in the rotational differential cross section around the low Δj rotational levels. Although we predicted that the rotational differential cross section would not curve significantly over its energy level spacing at

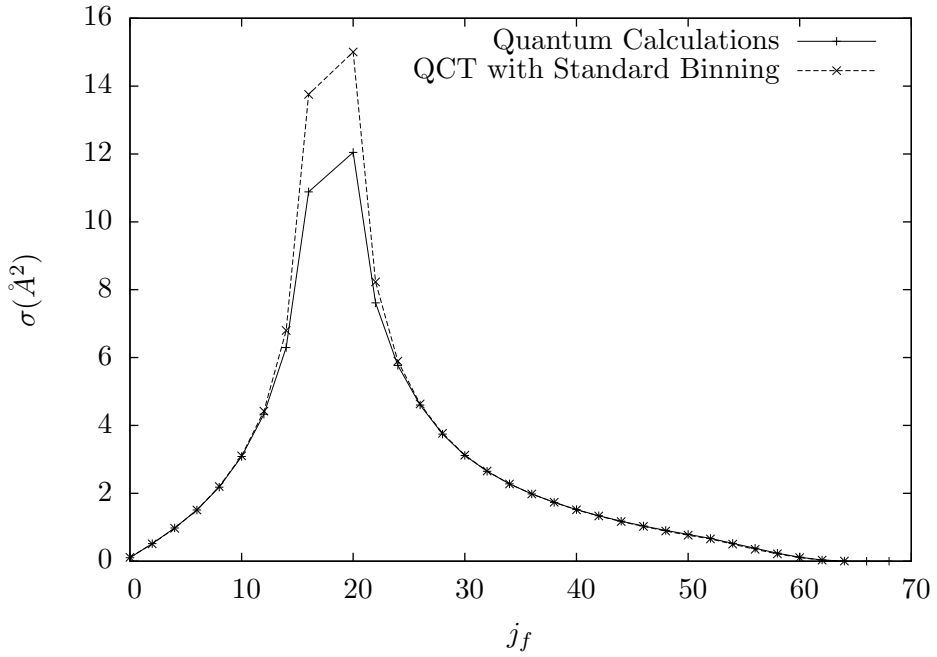

FIGURE 3.2: Vibrationally elastic cross sections as a function of final rotational quantum number at 2500 cm^{-1} using the QCT with standard binning and Quantum Mechanics

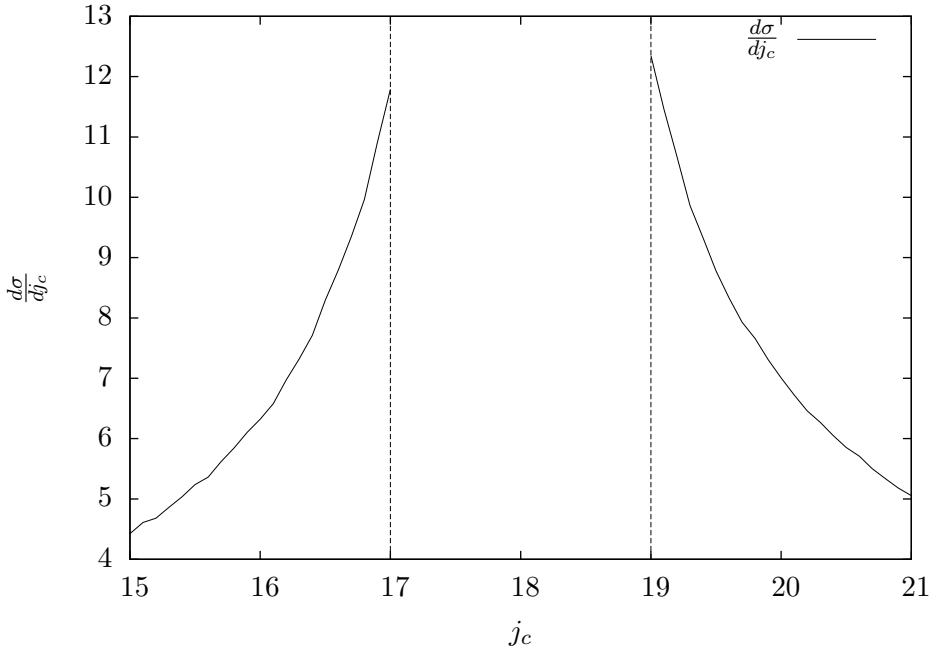

FIGURE 3.3: Rotational differential cross section plotted for $j_c > 17$ and $j_c < 19$

$2500cm^{-1}$, there clearly an exception in the $\Delta j = \pm 2$ range. We see this exception because the collisions that are close to being rotationally elastic usually occur when the atom hits the molecule nearly perpendicular to the bond. Since this right angle is the most likely angle that the atom will see as it approaches the molecule, the distribution of rotational actions sees a sharp peak at the rotationally elastic point [Stewart et al. [25]].

In order to see if the disagreement between the QCT with standard binning and quantum mechanics is due to this non-linearity, we compare the standard binning collision cross section with the rotational differential cross section, calculated using standard binning in vibration. As indicated by Equation 1.24, the rotationally delta-function binned cross section will be equal to twice the rotational differential cross section evaluated at the allowed quantum numbers. When we calculate the rotationally delta-function binned cross section in this manner, we see improved agreement with quantum mechanics (Figure 3.4).

At low Δj, the QCT with standard binning disagrees with quantum mechanics because it **counts a disproportionate number of trajectories that are classically more rotationally elastic than their quantum number would indicate**. This finding leads us to consider that the rest of the disagreement may be due to an incorrect quantization of the vibrational action. In order to test this, we apply gaussian binning to both the rotational and vibrational action. When we implement this procedure, we find that the vibrationally elastic cross section is highly dependent upon the FWHM of the gaussian binning function. (Figure 3.5)

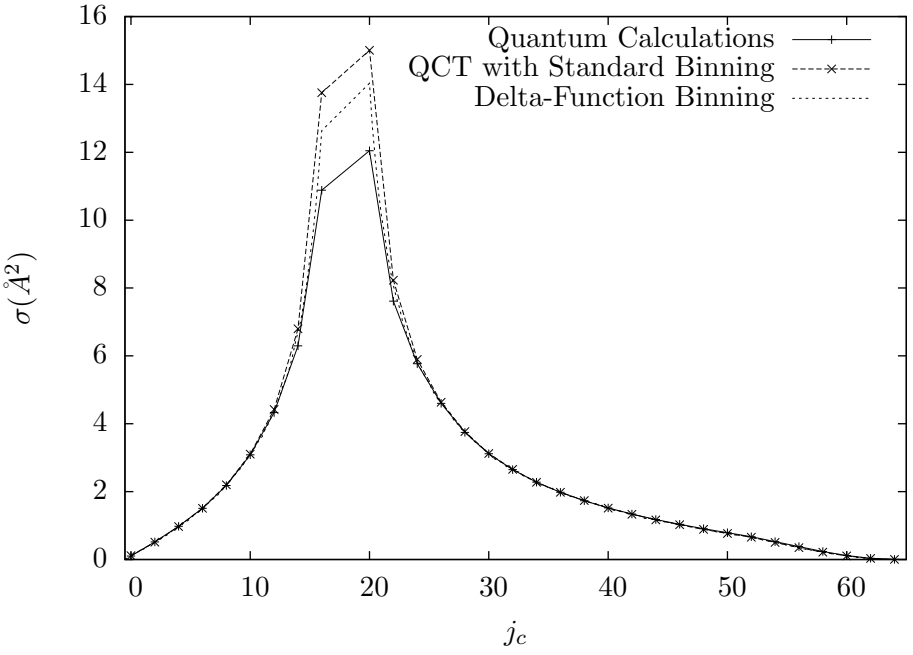

FIGURE 3.4: Comparison between the vibrationally elastic cross sections calculated using quantum mechanics, QCT with standard binning and delta-function binning in rotation for a variety of final rotational states

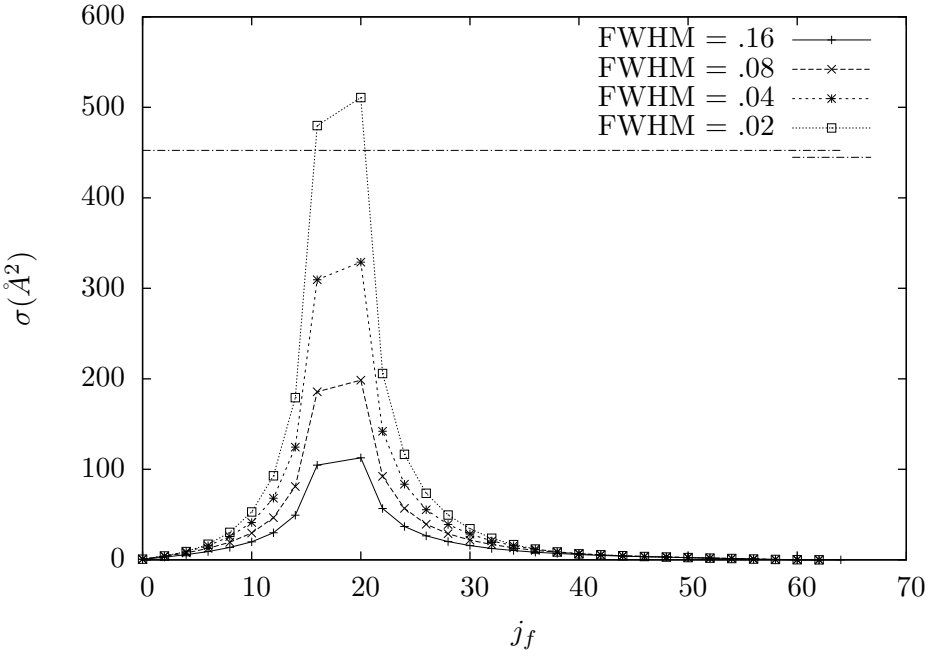

FIGURE 3.5: Vibrationally Elastic Cross Section as a function of final rotational quantum number at 2500 cm^{-1} using gaussian binning with a variety of different full-width-half-maxes. The quantity πb_{max}^2 is indicated by the horizontal line.

In fact, when the bin width is shrunk past a specific point, these vibrationally elastic cross sections begin to exceed the area of the disk drawn out by our maximum impact parameter, which is chosen to incorporate all inelastic collisions. The cross sections that exceed πb_{max}^2 imply that more than 100% of the trajectories sampled over the area πb_{max}^2 will reach a final quantum number, an obvious contradiction.

While narrow-width binning in rotation improves the agreement with quantum mechanics, narrow-width binning in vibration leads causes the cross section to greatly overestimate the quantum mechanical result. We see this because the vibrational differential cross section overlaps significantly with the vibrational binning functions at the $(v_f = 0,\ j_f)$ quantum numbers (Figure 3.6).

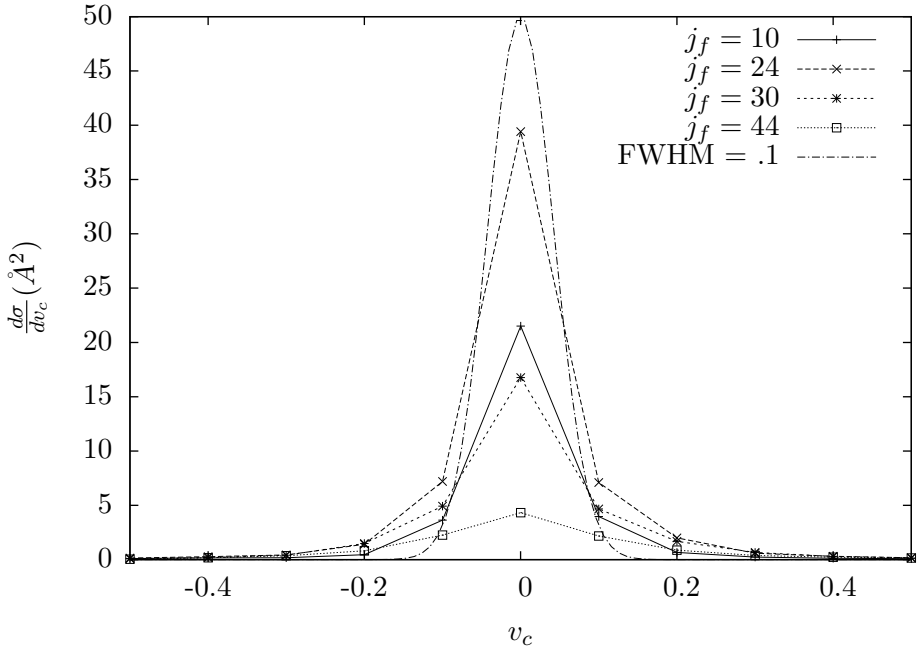

FIGURE 3.6: Vibrational differential cross section in the vibrationally elastic standard bin, calculated at various final rotational quantum numbers. A gaussian with FWHM = .1 of arbitrary height is superimposed

As a result of this overlap, the intregrand in Equation 1.11 will be extremely large for very low values of $|v_c|$. As we argued on Page 9 of Chapter 1, the dependence

of the collision cross sections on their binning functions is solely a function of the overlap between the differential cross sections and the binning functions. Since the overlap between the vibrational differential cross section and the vibrational binning function will always increase as the FWHM of the binning curve is decreased, the collision cross section will increase monotonically as the bin width is shrunk within our signal range.

When we use the typical FWHM for gaussian binning of 10% of a bin width, we find collision cross sections that are an order of magnitude larger than the standard binning cross sections. As mentioned in the introduction, Bonnet and Rayez deal with this problem by using whichever method, between gaussian and standard binning, produces the smaller cross section at a particular quantum number. This treatment allows one to extract most the benefits from gaussian binning, while avoiding the major pitfalls. However, **we do not believe that gaussian binning is always wrong when it predicts a smaller cross section than standard binning.** Later in the study, we will demonstrate a scenario where gaussian binning predicts larger cross sections than standard binning, and is also more classically correct. As a result of this consideration, we argue that **gaussian binning can be used within a degree of freedom as long as the derivative of the cross section with respect to its classical action can be made to converge.** Luckily, when the gaussian binning cross section increases monotonically as the bin width is shrunk, the vibrational differential cross section is narrowly peaked. In this case, standard binning satisfies the quantization condition very well. We will show later in the paper.

For vibrationally elastic scattering at 2500 cm^{-1} on the ($v_i = 0,\ j_i = 18$) state, standard binning does a good job predicting the vibrationally elastic collision cross sections. This is unsurprising because this collision energy is much larger than the energy level spacing for rotational levels. In the few cases where standard binning overestimates the quantum cross section, we can improve the agreement by binning the rotational action using a narrow-width curve. However, when we attempt to calculate the vibrational differential cross section at $v_f = 0$, we are unable to find a convergent value before our data gets noisy. We conclude that for vibrationally elastic scattering, the QCT agrees best with quantum mechanics when standard binning is used on the vibrational action, and some form of narrow-width binning is used on the rotational action.

3.3.1 Vibrationally Inelastic Collisions

We now examine the effects of gaussian binning on vibrationally inelastic scattering. While excitations to vibrational level $v_f = 2$ are possible, they are highly unlikely. Even when we utilize 10^9 trajectories at a collision energy of 2500 cm^{-1}, we are not able to calculate meaningful cross section using narrow-width binning methods. We instead examine trajectories that land at $v_f = 1$, which are much more probable and provide a more robust area to examine the effects of binning. Despite the fact that our system has a small de Broglie wavelength, we see significant disagreement between classical and quantum calculations. (Figure 3.7)

Standard binning overestimates the $\Delta v = 1$ collision cross section at all j_f, but agrees especially badly in two areas: $j_f \approx 18$ and $j_f \approx 50$. This phenomenon, in

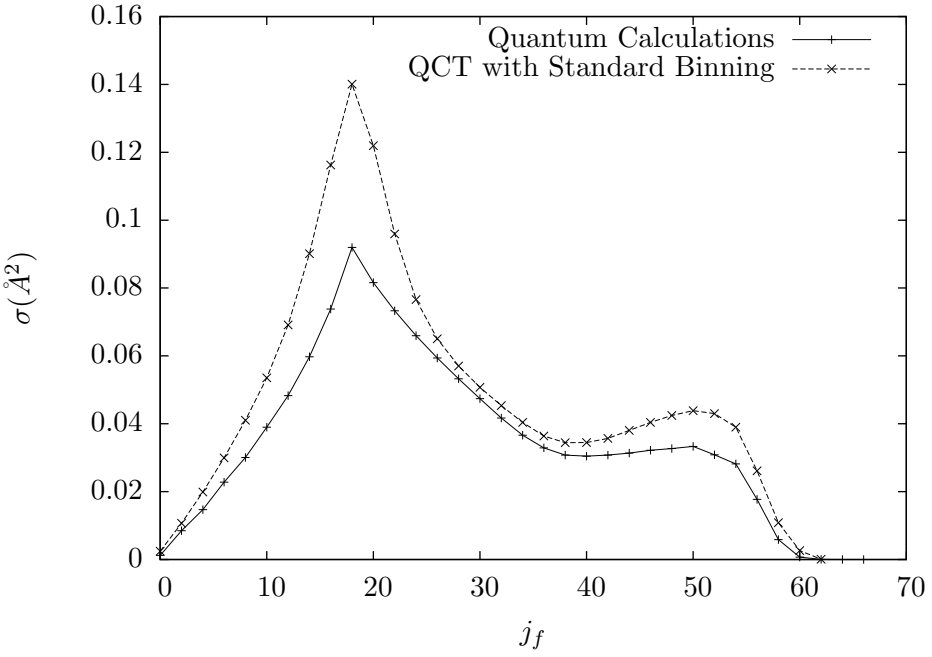

FIGURE 3.7: Collision cross sections as a function of j_f for $v_f = 1$ using quantum mechanics and the QCT with standard binning

which standard binning does not correctly account for vibrational energy transfer, has been seen in other systems with many vibrational modes. Gaussian binning has been shown to correct for these issues, giving vibrational branching ratios and rotational distributions that better agree with quantum mechanics [Banares et al. [1, 18]]. However, we find that in the Li_2 + Ne system, gaussian binning fails to improve the agreement of the rotational distribution (Figure 3.8).

While gaussian binning generally predicts less vibrational energy transfer, the cross sections are reduced from the rotational states for which standard binning agrees relatively well. More distressingly, the large peak around the rotationally elastic point, where standard binning fails most egregiously, remains unaffected. In order to shed light on this result, we model the vibrational differential cross section as a power law.

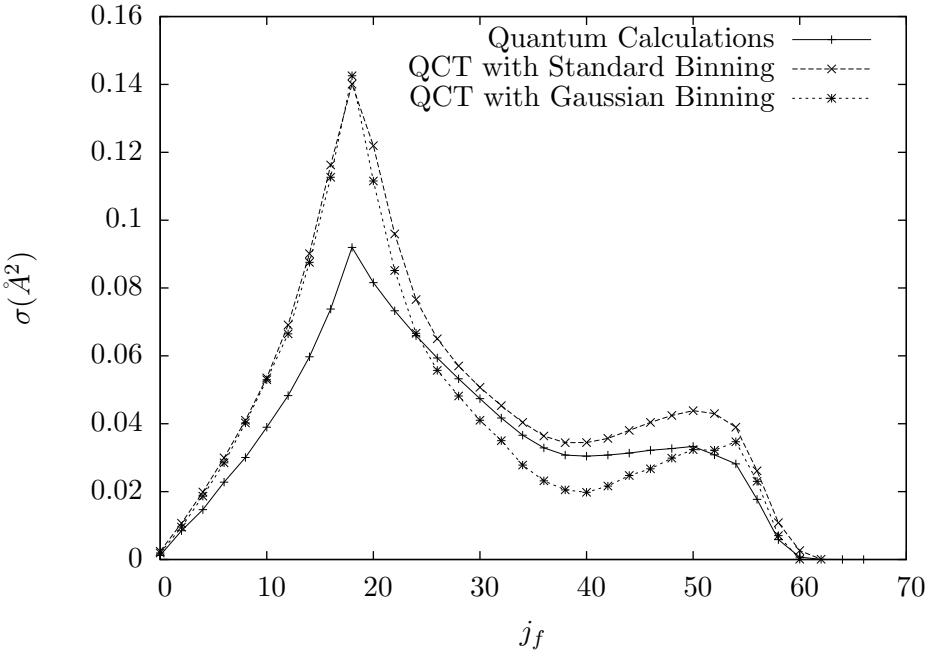

FIGURE 3.8: Collision cross sections as a function of j_f for $v_f = 1$ using quantum mechanics, the QCT with standard binning, and the QCT with gaussian binning

For rotational de-excitation, $\Delta j_f \leq 0$, the vibrational differential cross sections can be separated into three different regions where they obey distinct scaling laws. In the vibrationally elastic standard bin, $-.5 < v_c < .5$, the vibrational differential cross sections steeply drop off as a large negative power law, $\frac{\partial \sigma}{\partial v_c} \propto v_c^{-2.3}$ which abruptly becomes more gentle, $\frac{\partial \sigma}{\partial v_c} \propto v_c^{-.6}$ in the v = 1 bin, $.5 < v_c < 1.5$. Finally for $v_c > 1.5$ the vibrational differential cross section drops off extremely sharply. (Figure 3.9) While the vibrational differential cross section is more nuanced for rotational excitation, $\Delta j_f > 0$, the decay can also be approximately modeled by a power law, $\frac{\partial \sigma}{\partial v_c} \propto v_c^{-2}$ for $.1 < v_c < 1.5$. (Figure 3.10).

Using the rough functional relationship shown in Figures 3.9 and 3.10, and using Equation 1.27 to model delta function binning, gaussian binning in its ideal form, we estimate the ratio between the narrow-width binning cross section and the standard

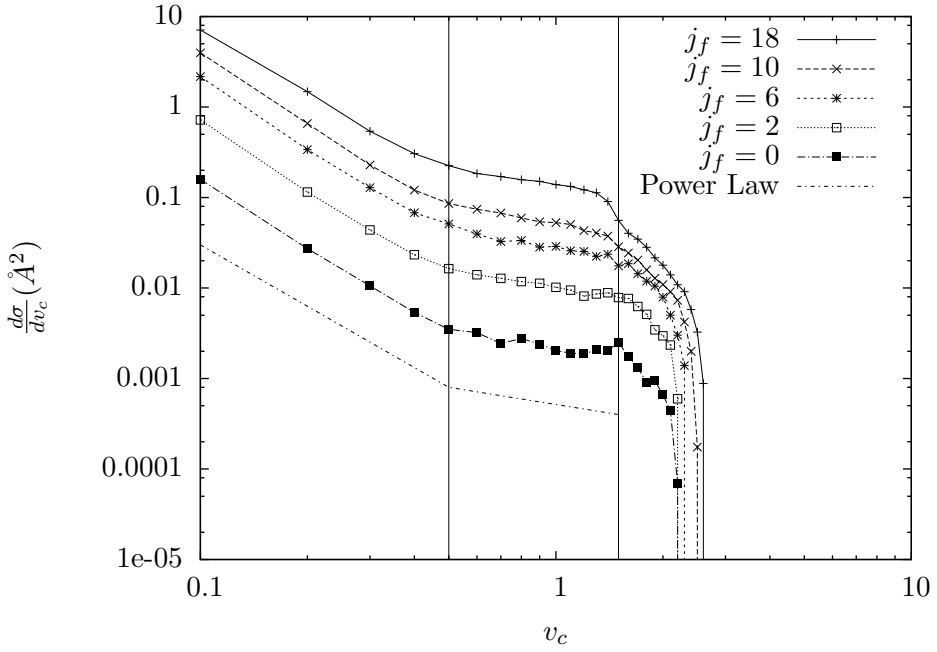

FIGURE 3.9: Vibrational differential cross section for various rotational de-excitations $j_f \leq 18$ on a log-log plot. The lowest line models the approximate power law dependence of the decay

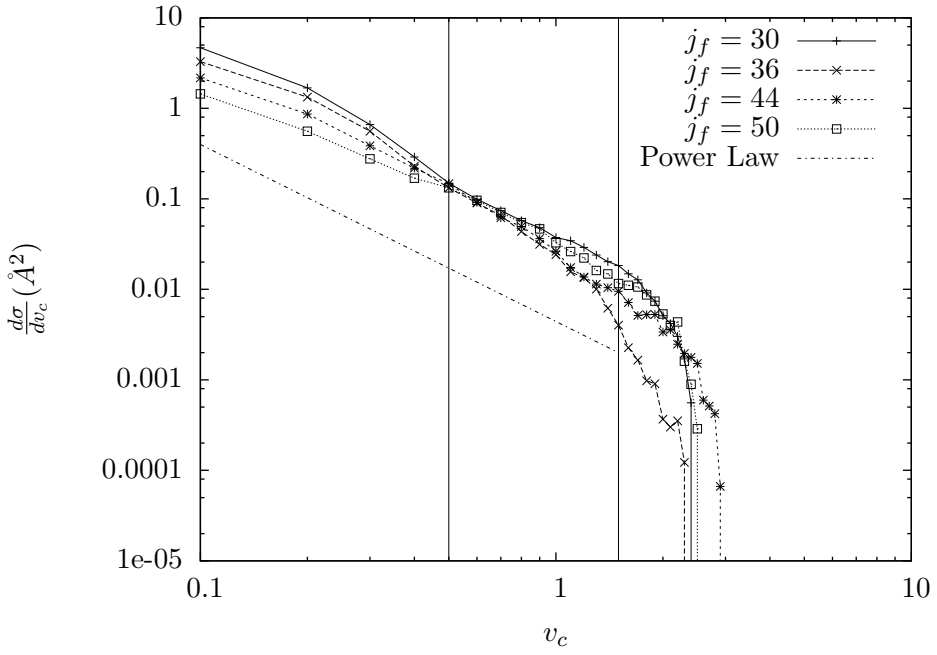

FIGURE 3.10: Vibrational differential cross sections for various rotational de-excitations $j_f > 18$ on a log-log plot. The lowest line models the approximate power law dependence of the decay

binning cross section for $\Delta v = 1$ processes. Since the vibrational differential cross section drops off much more sharply for rotational excitations $\Delta j > 0$, it will curve much more in the vibrationally inelastic bin and the ratio between delta-function binning and standard binning will be smaller. For vibrationally inelastic collisions, these ratios are approximately

$$\frac{\sigma_{db}}{\sigma_{sb}} \approx \begin{cases} .956 & \Delta j \leq 0, \\ .750 & \Delta j > 0. \end{cases} \tag{3.2}$$

While delta-function binning and standard binning give fairly similar results for rotational de-excitation, they diverge significantly for rotational excitation. So although gaussian binning reduces the vibrationally inelastic cross sections, it does not do so in a way that agrees well with quantum mechanics. Still, gaussian binning does predict the overall vibrationally inelastic cross section much more closely.

method	total vibrationally inelastic cross section
quantum mechanics	1.1872
standard binning	$1.88389 \pm .020373$
gaussian binning	$1.32845 \pm .01751$

3.3.2 Comments on Results

We find that **gaussian binning is useful for predicting overall vibrational excitation at** 2500 **cm^{-1}, but less useful for predicting the way that it**

is distributed among rotational states. Furthermore, we show that using a narrow-width binning method in the vibrationally elastic channel produces meaningless results because the trajectories with small $|\Delta v_c|$ are overweighted. Finally, we find that conducting narrow-width binning in rotation and standard binning in vibration produces optimal agreement with quantum mechanics.

In this section, we have shown that narrow-width binning methods have the ability to improve the rovibrational state distributions of the QCT when they are used judiciously. At the same time, we find that narrow-width binning methods can produce meaningless results when they are used under the wrong conditions. In Chapter 5 of this paper, we will attempt to make a set of theoretical guidelines in order to justify the selective use of gaussian binning and other narrow-width binning methods, provided certain conditions are met. For now we move on to the symmetrical windowing method, which we hope will help the quasi-classical trajectory method better agree with quantum mechanics at threshold.

Chapter 4

Symmetrical Windowing and Threshold Behavior

4.1 Introduction

In the previous chapter we investigated collisions at a total energy of 2500 cm^{-1}, at which the de Broglie wavelength is negligibly small. Most of the transitions at 2500 cm^{-1} were away from threshold, as we chose an energy that was about double the classical threshold for vibrational excitation, $E_{th} \approx 1300\ cm^{-1}$. In this chapter we shift our focus to energies 440 $cm^{-1} < E_{coll} < 1300\ cm^{-1}$, for which quantum mechanics predicts vibrationally inelastic transitions but classical mechanics does not. In order to understand this threshold chasm better, we examine the energy dependence of the QCT cross section for a variety of rovibrational transitions in an attempt to find good agreement with quantum mechanics.

4.2 Agreement Between Symmetrical Windowing and Quantum Mechanics

At 2500 cm^{-1}, much of the disagreement between classical and quantum mechanics is due to the quantization condition that quantum mechanics imposes. However, at energies closer to the threshold for vibrational excitation, it is likely that tunneling effects will cause significant disagreement as well. We expect that gaussian binning, which attempts to bin trajectories in the most classically correct way, will be unable to remedy the divergence between classical and quantum methods near threshold. As a result, in this chapter we will examine the symmetrical windowing method proposed by Cotton and Miller [Cotton and Miller [14]] most closely, as it has been able to improve upon the threshold behavior of classical mechanics for $H + H_2$ reactions in one dimension [Cotton and Miller [14]]. We find that while symmetrical windowing does smooth the threshold of vibrational excitation slightly, it is unable to fully mimic the threshold of quantum mechanics, even when we increase the windowing width past the suggestion of Cotton and Miller. Additionally, when we do increase the width on the symmetrical windowing processes, we tend to severely overestimate the vibrationally inelastic cross sections at higher energies. Finally, we find that for vibrationally elastic collisions, symmetrical windowing engenders similar problems to those of gaussian binning by overweighting the dense channel of classically vibrationally elastic trajectories.

4.2.1 Vibrationally Elastic Collisions

We begin by testing symmetrical windowing on vibrationally elastic collisions. For these cross sections, standard binning agrees extremely well with quantum mechanics at high energies. At lower energies the cross-sections begin to diverge as quantum effects become more important (Figure 4.1).

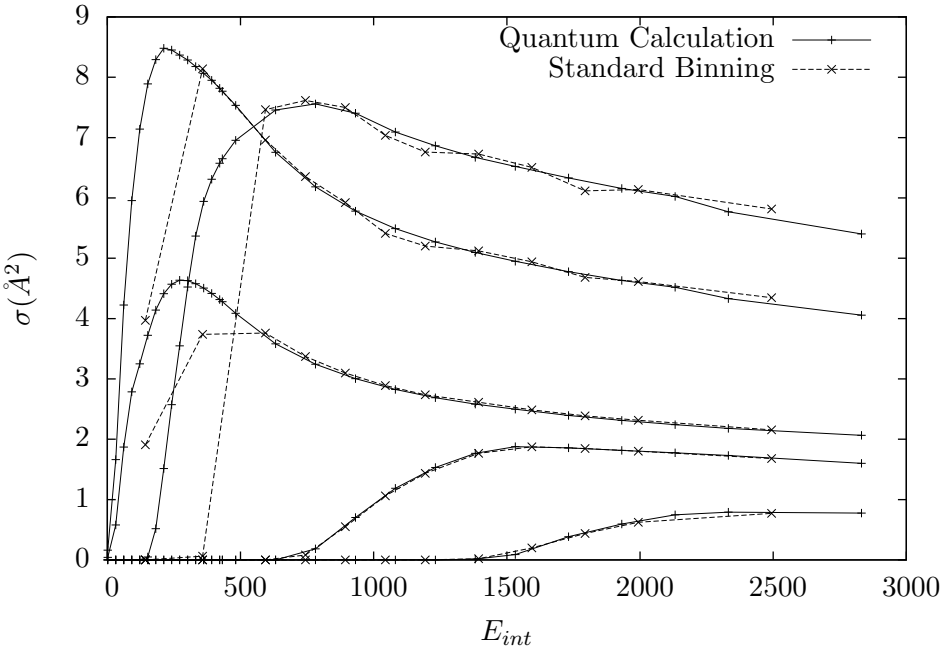

FIGURE 4.1: Comparison between quantum mechanical calculations and QCT with standard binning for vibrationally elastic cross sections as a function of energy, for transitions $(v_i = 0, j_i = 18) \rightarrow (v_f = 0, j_f)$ where $j_f = 24, 12, 8, 38, 50$ from top to bottom

Unfortunately, symmetrical windowing is unable to replicate the good agreement of standard binning, as it gravely overestimates the vibrationally elastic cross sections at all energies. Furthermore, when the width of the windowing function is narrowed, the disagreement is worsened (Figure 4.2).

The magnitude of the cross section is inversely related to the width of the symmetrical windowing curve. This idea is supported by the enormous value of the gaussian

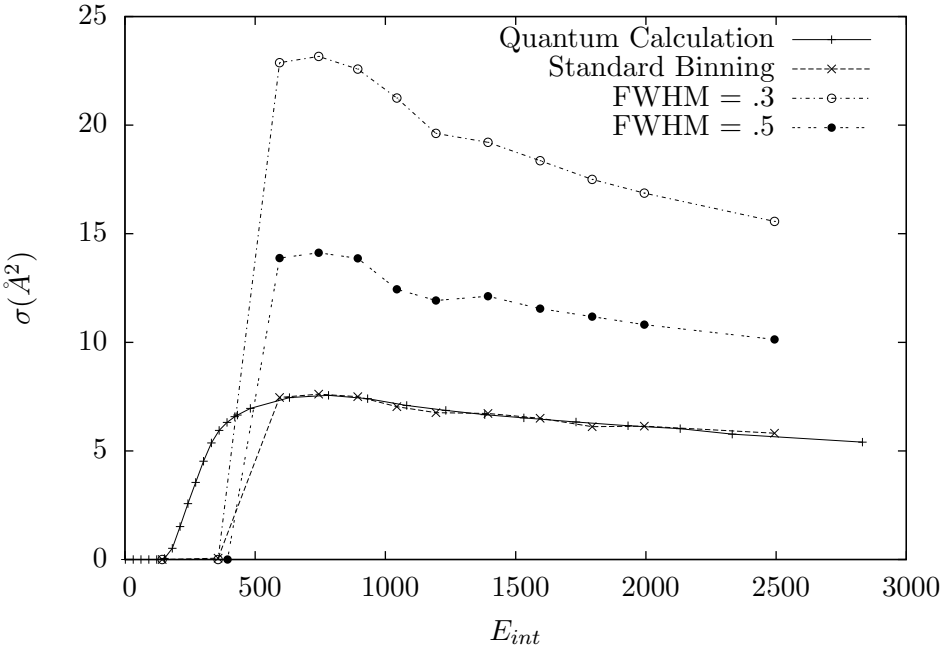

FIGURE 4.2: Comparison of quantum mechanical calculations, the QCT with standard binning, and symmetrical windowing with a full-width-half-max of .3 and .5 for vibrationally elastic cross sections as a function of energy, for the transition $(v_i = 0, j_i = 18) \rightarrow (v_f = 0, j_f = 24)$

binned vibrationally elastic cross section (Chapter 2), as gaussian binning could be thought of as symmetrical windowing with a narrow width.

Even though symmetrical windowing samples the initial actions over a distribution, the overwhelming majority of trajectories are still classically vibrationally elastic. As a result of this, the distribution of final vibrational actions heavily resembles the distribution of initial vibrational actions. Even when the FWHM is set to half a bin width, the overlap between the binning curve and the final distribution is severe enough to make the cross sections extremely large.

4.2.2 Vibrationally Inelastic Collisions

We now test symmetrical windowing on vibrationally elastic collisions, the regime where we would most realistically expect it to improve agreement. While the symmetrical windowing process has not been tested on inelastic scattering before, it has been shown to improve agreement at the threshold of a reaction [Cotton and Miller [14]]. As a argued by Cotton and Miller, the symmetrical windowing method works nicely near threshold because it makes some energy transitions easier while making other energy transitions more difficult. For example, with a FWHM = .5, there is an 11% chance the symmetrical windowing method will sample a trajectory with ($v_c > .25,\ E - E_{v_i} > 64\ \text{cm}^{-1}$) and an 11% chance that symmetrical windowing will sample a trajectory with ($v_c < -.25,\ E - E_{v_i} < -64\ \text{cm}^{-1}$). Away from threshold, the effect of giving some of the trajectories extra energy and internuclear momentum should be offset by the effect of subtracting energy from other trajectories. However, near a threshold that the majority of trajectories are unable to pass, the effect of increasing the initial energy of some trajectories should outweigh the effect of decreasing the internal energies of others, as it should add variance to the final energy of the diatom.

Unfortunately, contrary to our predictions, symmetrical windowing does not improve upon the agreement of standard binning, for the majority of transitions within the threshold region. (Figure 4.3 and 4.4).

As can be seen, none of the quasi-classical methods are able to mimic the gentle quantum mechanical threshold. Instead the QCT methods have a much stronger

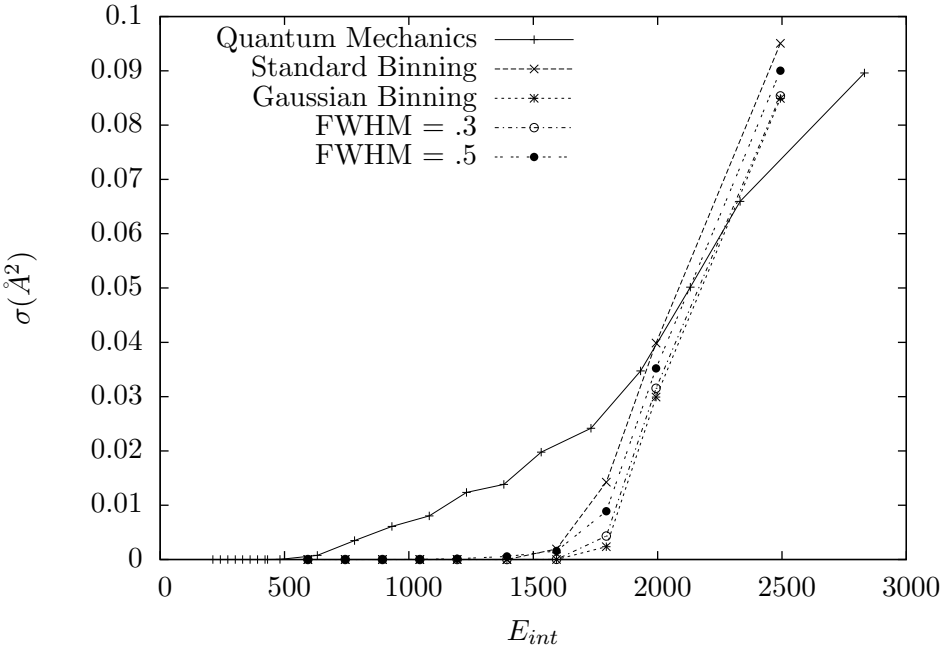

FIGURE 4.3: Collision cross sections as a function of collision energy for $(v_i = 0, j_i = 18) \rightarrow (v_f = 1, j_f = 24)$ using standard binning, gaussian binning, symmetrical windowing and quantum mechanics

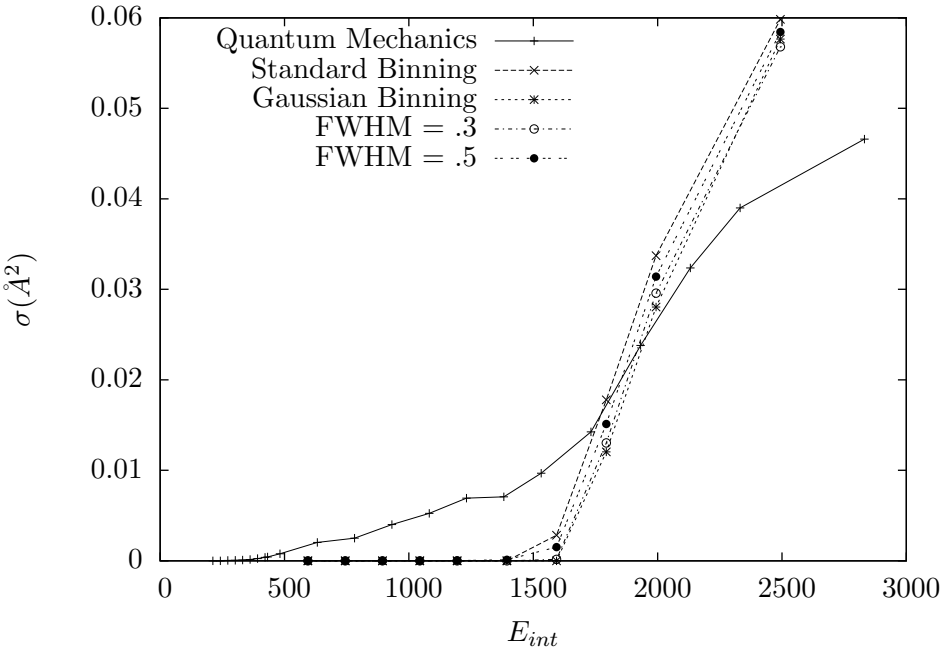

FIGURE 4.4: Collision cross sections as a function of collision energy for $(v_i = 0, j_i = 18) \rightarrow (v_f = 1, j_f = 10)$ using standard binning, gaussian binning, symmetrical windowing and quantum mechanics

energy dependence, delivering larger cross sections at high energies, and dropping off to zero at much higher energies than the threshold energy of the quantum cross sections. Unsurprisingly, gaussian binning has the largest threshold energy, as it effectively only samples classical trajectories that make the full vibrational transition, $\Delta v_c = 1$. More surprisingly, the symmetrical windowing methods still reach threshold at a higher energy than standard binning. Even when the FWHM is increased from 30% of a bin-width to 50% the threshold remains higher than standard binning. As it turns out, standard binning is already very good at allowing $\Delta v_c < 1$ transitions to occur, as any trajectory with $v_c > .5$ is counted towards the $v_f = 1$ state. **We find that the larger effective binning width of standard binning is enough to override the increased variance induced by the initial sampling of symmetrical windowing.**

Interestingly, at higher j_f, the quantum mechanical threshold energy becomes much larger, and the cross-section takes on a much stronger energy dependence. For these Δj large transitions, the quasi-classical trajectory method does a much better job at predicting quantum mechanics. For example, at $j_f = 44$ the symmetrical windowing method with a FWHM of half a bin width does a very good job modeling the quantum mechanical cross section (Figure 4.5)

4.3 Conclusions

For all three of the transitions that we have shown, the quasi-classical cross sections have a positive linear dependence on collisional energy and a threshold energy of

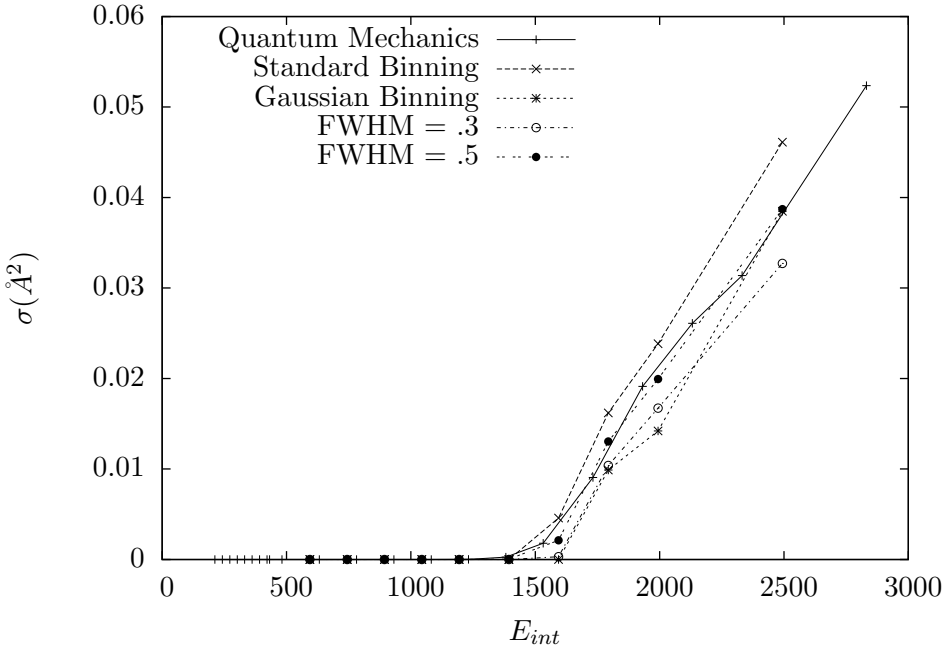

FIGURE 4.5: Collision cross sections as a function of collision energy for $(v_i = 0, j_i = 18) \rightarrow (v_f = 1, j_f = 44)$ sing standard binning, gaussian binning, symmetrical windowing and quantum mechanics

around 1300 cm^{-1}. Additionally, these quasi-classical curves can be shifted towards a slightly lower threshold energy through using a wider width binning method, such as wide width symmetrical windowing or standard binning. While symmetrical windowing methods with FWHM = .5 and FWHM = .3 were are able to shift the threshold slightly, standard binning was shown to have the largest effect. However, at low j_f, none of the quasi-classical techniques are able to induce agreement with quantum mechanics, as the quantum threshold is far less steep, and extends to a far lower energy than the classical one.

As j_f is increased, the quantum mechanical thresholds become steeper, eventually reaching a point where they can be modeled effectively by classical mechanics. In the example of $j_f = 44$, the quantum mechanical cross section can be closely modeled by the symmetrical windowing method with a FWHM of half a bin width. However,

based on the agreement of symmetrical windowing at other j_f, we view this agreement as a fortuitous coincidence, and certainly not a generalizable trend. Still, the presence of such an agreement leads us to wonder if symmetrical windowing may be an effective model for describing thresholds in regions that behave more classically.

As we have seen, gaussian binning, symmetrical windowing, and standard binning are all useful for modeling quantum mechanics in some situations, but fail to provide accurate models in others. Now that we have figured out when these methods work best, we would like to make a judgement about when they are most theoretically valid. In order to do so we turn to microscopic reversibility [Polanyi and Schreiber [29]], which is a condition that must be satisfied for a time-reversible process. Through figuring out when these methods are most microscopically reversible, we can figure out when they best obey the laws of classical mechanics, and hopefully create some guidelines for choosing the proper QCT method.

Chapter 5

Microscopic Reversibility

In order to test whether the QCT methods we have discussed thus far satisfy time reversal symmetry, we test microscopic reversibility [Polanyi and Schreiber [29]] at a total energy of 2500 cm^{-1}. The microscopic reversibility constant (MRC) for the trajectories that travel from quantum number (v_i, j_i) to quantum number (v_f, j_f), is calculated using the following equation

$$MRC = \frac{\sigma_{v_i,j_i \to v_f,j_f}(E_t - E_{v_i,j_i})(2j_1 + 1)}{\sigma_{v_f,j_f \to v_i,j_i}(E_t - E_{v_f,j_f})(2j_f + 1)}. \tag{5.1}$$

We study these constants at 2500 cm^{-1} because it is large enough energy to allow for a significant number of trajectories to undergo vibrational excitation. As a result, we are able to calculate the microscopic reversibility constants for both vibrationally elastic processes $(v_i = 0,\ j_i = 18) \to (v_f = 0,\ j_f)$ and vibrationally inelastic processes $(v_i = 0,\ j_i = 18) \to (v_f = 1\ j_f)$, with relatively small error bars. Since each microscopic reversibility constant requires two cross sections that begin at $(v_i,\ j_i)$

and (v_f j_f), we only calculate these microscopic reversibility constants for a variety of selected j_i and j_f . The following table lists the collision cross sections and the number of trajectories we used to calculate them.

j_i	0	10	18	24	30	36	44	54
N	10^8	$8.6X10^7$	$1.2X10^7$	$1.6X10^7$	$4.6X10^7$	10^8	10^8	$2.5X10^7$

5.1 Wide-Width vs. Narrow-Width Binning

As we argued in the introduction, the condition of microscopic reversibility is related to the symmetry between the initially sampled action distribution, $P(|v_f - v_c|, |j_f - j_c|)$, and the product of the classical differential cross section and the binning function, $\frac{1}{\pi b_{max}^2} \frac{\partial^2 \sigma}{\partial v_c \ \partial j_c} \ W(|v_f - v_c|, |j_f - j_c|)$. For the standard and gaussian binning methods, the initial classical actions are all set to equal the initial quantum number. In these cases, microscopic reversibility will be satisfied when the product of the binning curve and the classical differential cross section is narrowly peaked. In the limit of narrow width gaussian binning, i.e. delta-function binning, the collision process is perfectly symmetrical, as only trajectories that make a transition from one action to another are used to calculate the cross section. The forward process, for which all of the trajectories begin at the initial quantum number and end at the final quantum number, is symmetrical to the reverse process, for which all of the trajectories begin at exactly the final quantum number and end at exactly the initial quantum number.

However, as we will show, microscopic reversibility can be satisfied when a wider width binning function is used under certain conditions. As we showed in Chapter 1 (Equations 1.17 and 1.18), the cross section is independent of binning function when the differential cross sections are linear. The MRCs for a given $(v_i, j_i) \rightarrow (v_f, j_f)$ process are only dependent upon the calculation of the cross sections $(v_i,\ j_i) \rightarrow (v_f,\ j_f)$ and $(v_f,\ j_f) \rightarrow (v_i,\ j_i)$. As a result, a binning method will be microscopically reversible as long as these cross sections are equal to the cross sections of a microscopically reversible binning method. **When the vibrational and rotational differential cross sections are linear, the cross section calculated using any binning curve will be equal to the delta-function binned cross section, and therefore will be microscopically reversible**.

Additionally, a process will always be microscopically reversible within vibration/rotation when the vibrational/rotational differential cross section is narrowly peaked. In this case the product of the binning function and the differential cross section will be narrowly peaked, even if the binning function is not.

Microscopic reversibility is only violated when the vibrational/rotational differential cross section is non-linear, and its actions are binned using a wider-width binning method. In this case, the wider-width binning method will produce different cross sections than the delta-function binned cross sections and the MRCs may not be equal to unity.

5.2 Vibrationally Elastic Collisions

For vibrationally elastic collisions at 2500 cm^{-1} the quasi-classical trajectory method should always satisfy microscopically reversibility with respect to vibration, as the vibrational differential cross section is narrowly peaked. Furthermore, any QCT method should satisfy microscopic reversibility with respect to rotation, as the rotational differential cross section is generally linear on the scale of its quantum number separation at this energy. From these two considerations, we predict that the all of the binning methods should satisfy microscopic reversibility very well for vibrationally elastic collisions at 2500 cm^{-1}. As expected, for most j_f, standard binning, gaussian binning, and symmetrical windowing all produce microscopic reversibility constants that are reasonably close to one (Figure 5.1)

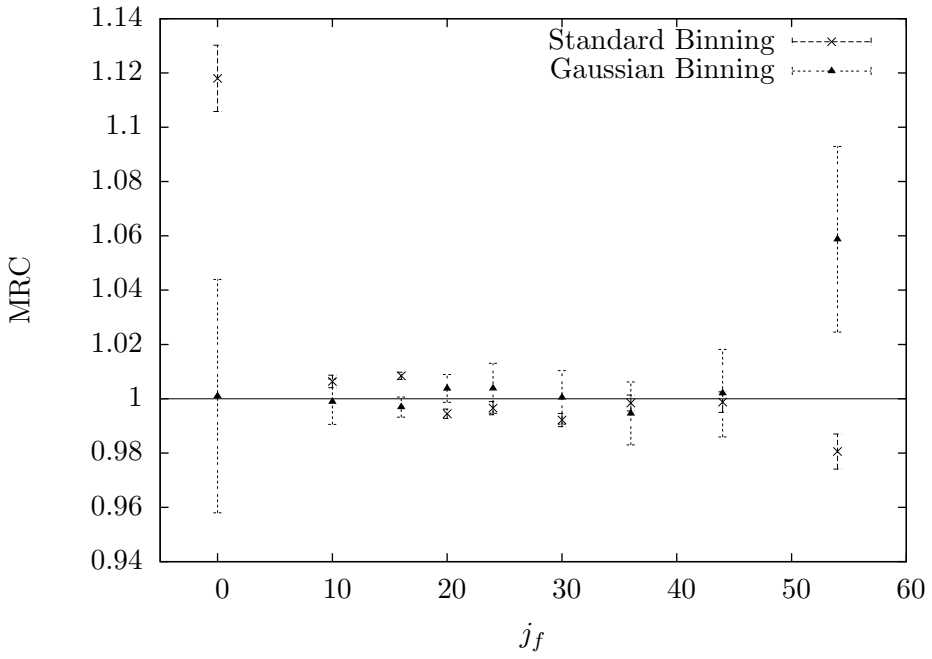

FIGURE 5.1: Microscopic reversibility constants for the process $(v_i = 0, j_i = 18) \rightarrow (v_f = 0, j_f)$ using standard binning and gaussian binning

Aside from gaussian binning for the $(v_i = 0, j_i = 18) \rightarrow (v_f = 0, j_f = 54)$ process, and the wider-width binning methods for the $(v_i = 0, j_i = 18) \rightarrow (v_i = 0, j_i = 0)$ process, all of the microscopic reversibility constants are within 5% of unity. We hypothesize that the large value of the gaussian binning MRC at $j_f = 54$ is due to statistical error, as the predicted constant is within two standard deviations of unity. However, we believe that the error in the wider-width binning methods for the $(v_i = 0, j_i = 18) \rightarrow (v_i = 0, j_i = 0)$ MRCs represents a true violation of microscopic reversibility.

As it turns out, this error is related to a flaw in the standard binning method for trajectories that land within the $j_f = 0$ standard bin. Our trajectory method uses the Langer approximation $E_j = \hbar^2 \ (j + \frac{1}{2})^2$. By implementing this approximation, we are able allow our classical action to take a minimum value of $j_c = -\frac{1}{2}$ throughout the course of the collision. However, since our atom is homo nuclear, the standard bin of the $j_f = 0$ state is two quantum numbers wide. As a result, the region of the standard bin from $j_c = -1$ to $j_c = -.5$ is always entirely empty. Even though the rotational differential cross section is a linear function, it cannot be linear over the entire standard bin because it reaches a value of zero at $j_c = -.5$ (Figure 5.2)

The standard binning cross section, calculated with $W(v_c, j_c) = 1$ over the standard bin, is equal to twice the average value of the rotational differential cross section. Meanwhile, the delta function cross section is just twice the differential rotational cross section evaluated at the allowed quantum number. Approximating the area under the curve in Figure 5.2 as a triangle, we find that $\sigma_{sb} = \frac{9}{8}\sigma_{db}$. Based on this result we would expect the $(v_i = 0, j_i = 18) \rightarrow (v_f = 0, j_f = 0)$ standard binning

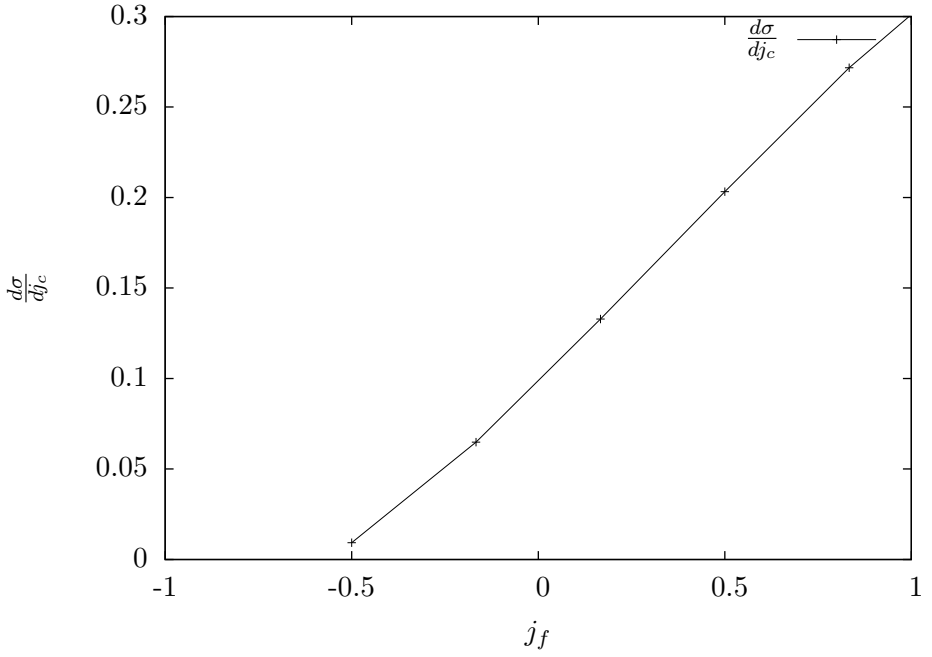

FIGURE 5.2: Rotational differential cross section inside the $j_f = 0$ standard bin

cross section to be too large by a factor of 10%. This is predicted by our MRC at $j_f = 0$ in Figure 5.1.

This error does not only occur for the cross section $(v_i = 0, j_i = 18) \rightarrow (v_f = 0, j_f = 0)$ but exists for all vibrationally elastic cross sections that reach the final state $j_f = 0$. These cross sections will be in the denominator of the microscopic reversibility constants of the processes $(v_i = 0, j_i = 0) \rightarrow (v_f = 0, j_f)$ (Figure 5.3).

Unsurprisingly, these microscopic reversibility constants are off by about 10% for standard binning. Despite this minor methodological error, which causes standard binning cross sections to be too large for states with $j_f = 0$, standard binning generally satisfies microscopic reversibility in the case of vibrationally elastic collisions.

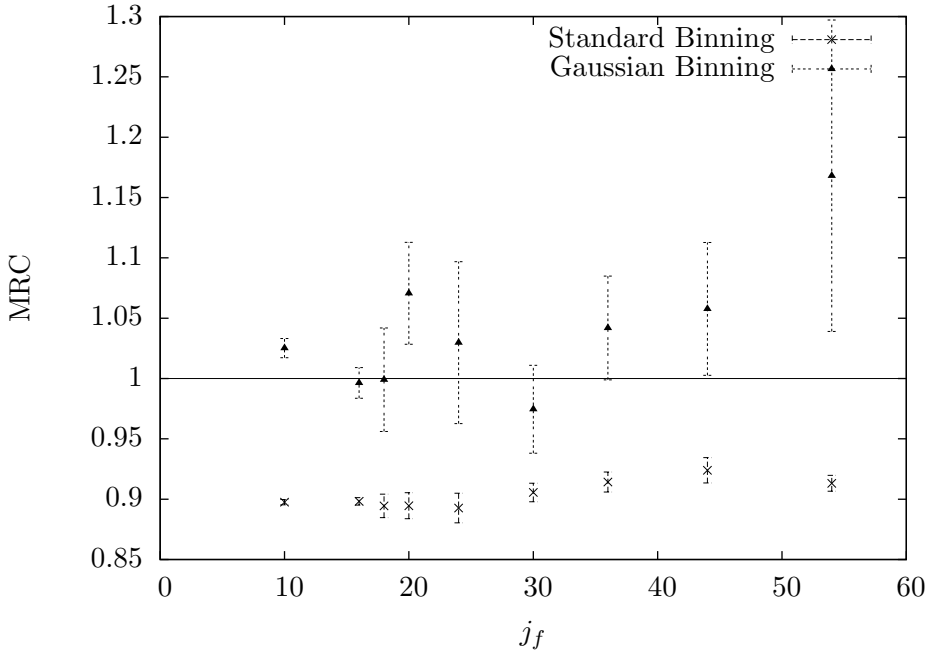

FIGURE 5.3: Microscopic reversibility constants for the process $(v_i = 0,\ j_i = 0) \rightarrow (v_f = 0,\ j_f)$ using standard and gaussian binning

5.3 Vibrationally Inelastic Collisions

We now turn to the case of vibrationally inelastic collisions where we expect standard binning to fare more poorly due to the non-linear vibrational differential cross sections. As predicted, standard binning does not fare as well for vibrationally inelastic collisions (Figure 5.4).

The standard binning microscopic reversibility constants show a clear trend, delivering results that are too large at low j_f, too small at intermediate j_f, before becoming too large again at high j_f. On the other hand the gaussian binning constants are distributed more randomly, and lie relatively close to within error. The systematic failure on the part of standard binning is a complex issue, but its source lies within the non-linearity of the vibrational differential cross section. In order to

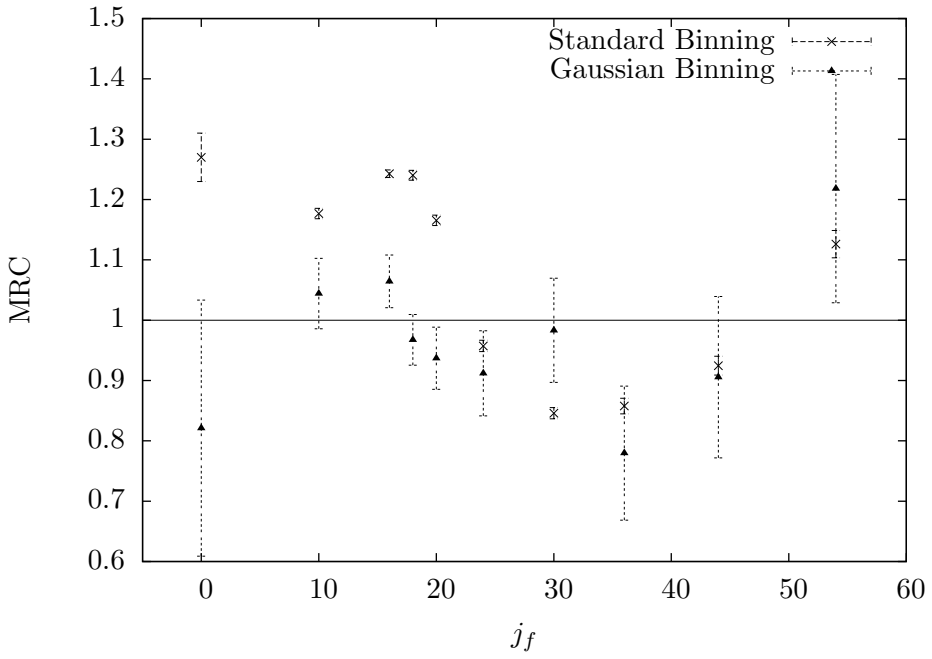

FIGURE 5.4: Microscopic reversibility constants for the process $(v_i = 0,\ j_i = 0) \rightarrow (v_f = 1,\ j_f)$ using standard and gaussian binning

further display the way that non-linearity affects the MRCs, we examine the case $\Delta v = 1,\ \Delta j \leq 18$, for which standard binning gives MRCs that are too large.

As demonstrated in Chapter 2, for cross sections of the form, $v_i = 0,\ j_i = 18 \rightarrow v_f = 1\ j_f \leq 18$, the vibrational differential cross section drops off as a weak power law, in such a way that the gaussian cross section is almost equal to the standard binning cross section (Figure 3.9, Equation 3.2). As a result we expect the inaccuracy in the standard binning MRCs to be due to an artificially small cross section for the reverse process.

For the reverse of these processes, $v_i = 1,\ j_i \leq 18 \rightarrow v_f = 0,\ j_f = 18$ the vibrational differential cross section plateaus from $v = .2$ to $v = -.2$ before dropping off to zero by $v_c = -.5$ (Figure 5.5).

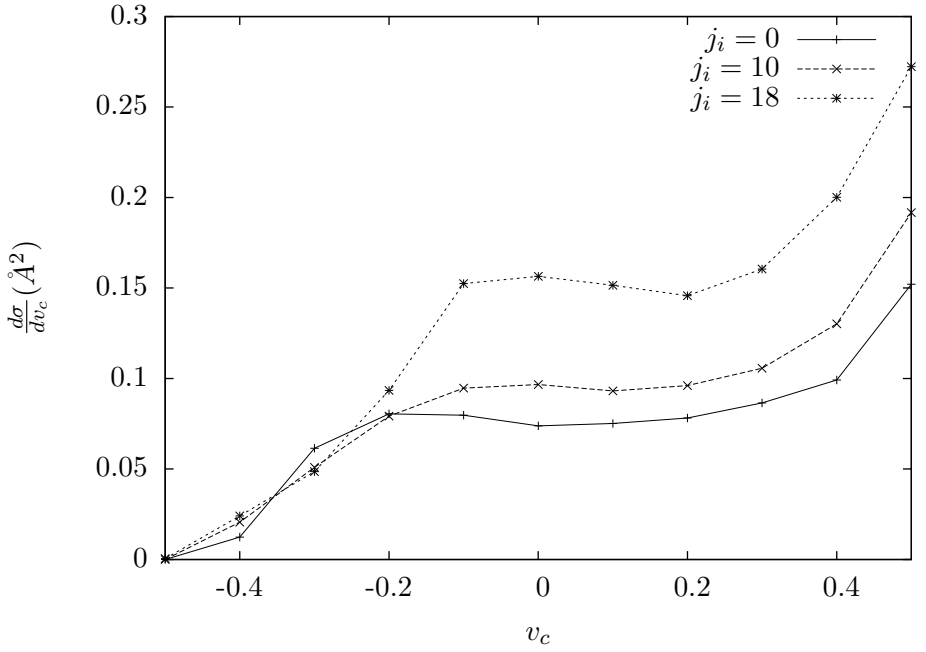

FIGURE 5.5: Vibrational differential cross section for the process $(v_i = 1,\ j_i) \rightarrow (v_f = 0,\ j_f = 18)$

We will call this shape of this vibrational differential cross section the two drop distribution, because there are two areas where the vibrational differential cross section increases as a function v_c separated by a plateau. Roughly speaking, if the drop on the negative v_c side is greater than the drop on the positive v_c side, standard binning will predict a smaller cross section than gaussian binning and vice versa. For these vibrational differential cross sections, the drop on the negative size appears to be larger, and as a result the gaussian binning cross sections are larger than the standard binning cross sections. This is also seen in our microscopic reversibility constants in Figure 4.4, as the gaussian binning MRC for the reverse of this process is smaller than the standard binning MRC.

Through this analysis we have stumbled upon an area where gaussian binning predicts a larger cross section than standard binning, but does not diverge, namely

transitions of the form $(v_i = 1\ j_i \leq 18) \rightarrow (v_f = 0,\ j_f = 18)$. Additionally, we know that gaussian binning is the more classically accurate method in this situation, as the MRC constants are within error of unity. In the introductory chapter, we mentioned that Bonnet and Rayez proposed that one should only use gaussian binning when it gives a smaller cross section than standard binning. Here, this criteria fails as the gaussian binned cross section is both classically correct and larger than the standard binning cross section.

The measured microscopic reversibility constants for collisions beginning $(v_i = 0, j_i = 18)$ state confirm our earlier hypothesis that narrow-width binning methods can ensure microscopic reversibility provided that the trajectories are not initially sampled. While the MRCs for gaussian binning were usually within 2σ of unity, the standard binning MRCs often deviated with a notable percent error. However, aside from a calculation quirk that resulted from the selection rules of Li_2, we found that standard binning in rotation does not cause a substantial failure in microscopic reversibility. Furthermore, we found that using standard binning in the vibrationally elastic channel is not problematic due to the narrowly peaked distribution of final vibrational actions.

As a result, we find that standard binning is only problematic for calculating vibrationally inelastic cross sections. In these situations, the curvature of the vibrational differential cross section causes the standard binning cross section to differ from the delta-function cross section by a non-negligible amount. Since delta-function processes which run from quantum number to quantum number are completely microscopically reversible, these deviations caused the standard binning MRCs to deviate

from unity.

5.4 Symmetrical Windowing

We now see if the symmetrical windowing processes satisfy microscopic reversibility. As we mentioned in the introduction, Cotton and Miller assert that symmetrical windowing is a microscopically reversible procedure because of the initially sampled distribution of classical actions is identical to the binning function. However, in the introduction we argued that a different kind of symmetry is required for microscopic reversibility, that the initial action distribution must resemble the product of the classical differential cross section and the binning function. As a result, we do not expect symmetrical windowing to be microscopically reversible in all cases.

For vibrationally elastic collisions, we expect the symmetrical windowing process to be microscopically reversible for the same reasons that the standard binning process is microscopically reversible. Since the distribution of rotational actions is linear, the method of binning the rotational actions should not have an effect on the cross section. Furthermore, the dense channel of trajectories in the vibrationally elastic bin ensures that the product of the vibrational differential cross section and the binning function will be symmetrical and narrowly peaked. While the distribution of initial vibrational actions has a larger spread than the weighted final distribution, both states are perfectly symmetrical with respect to the quantum number. As a result, we see that microscopic reversibility is satisfied very well for vibrationally elastic collisions. (Figure 5.6)

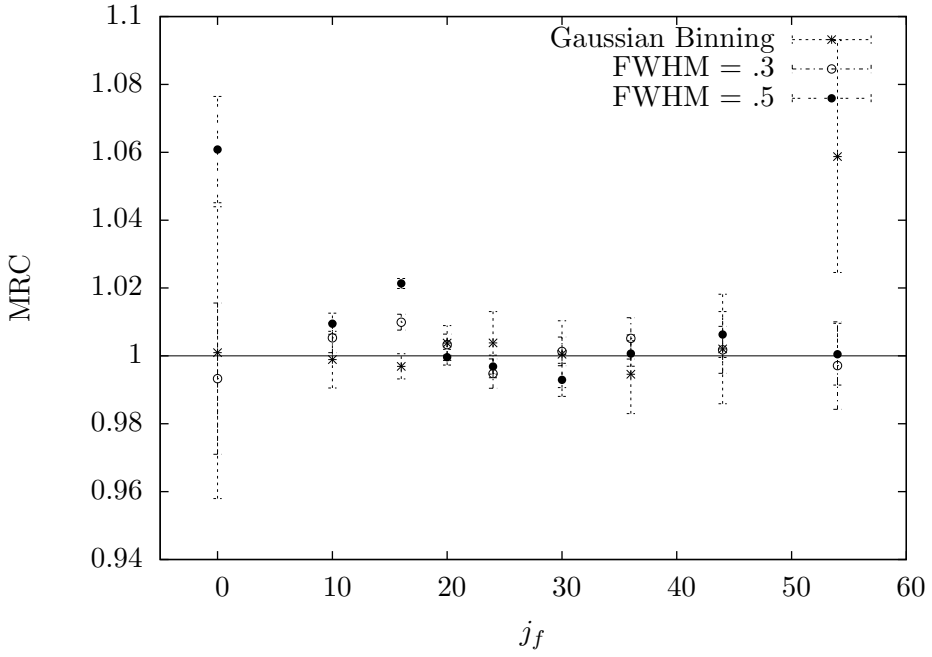

FIGURE 5.6: Microscopic reversibility constants for the process ($v_f = 0,\ j_f = 18) \rightarrow (v_f = 0,\ j_f$) using gaussian binning and symmetrical windowing.

For vibrationally inelastic collisions, the distribution of final vibrational actions is highly non linear within the $v_f = 1$ standard bin. As a result we would expect this non-linearity to upset the symmetry of the vibrational binning function, causing it to look different from the symmetrical distribution of initial vibrational actions. Indeed, we find that symmetrical windowing is not perfectly microscopically reversible for vibrationally inelastic collisions (Figure 5.7). As the FWHM of the windowing curve is increased, the percent error on the MRCs grow, as the wider width binning functions see more of the non-linearity in the vibrational differential cross section.

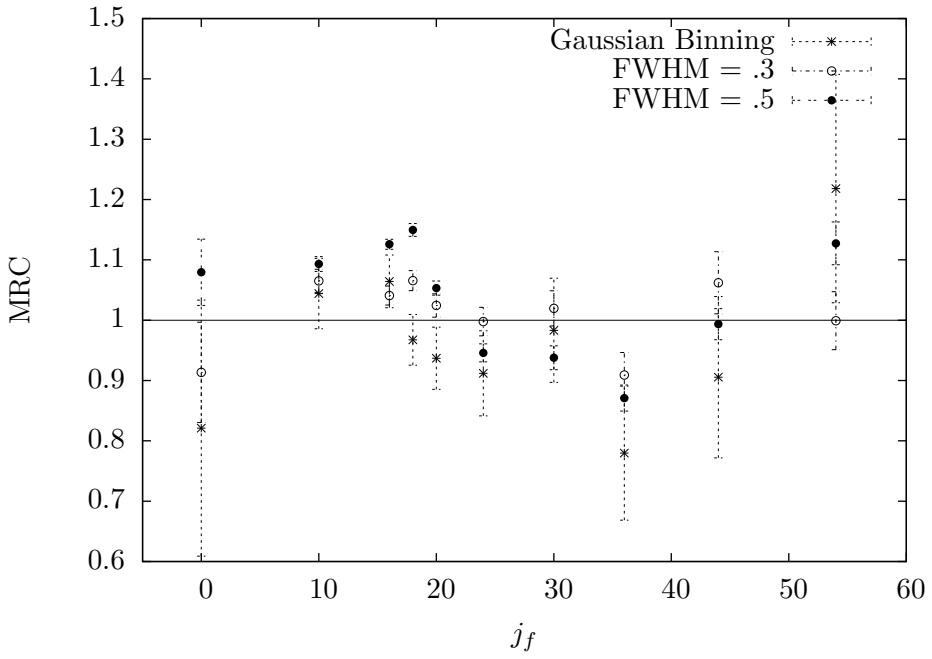

FIGURE 5.7: Microscopic reversibility constants for the process ($v_f = 0,\ j_f = 18$) $\rightarrow$ ($v_f = 1,\ j_f$) using gaussian binning and symmetrical windowing.

5.5 Conclusions

In this section, we have seen that the MRCs of symmetrical windowing processes behave much like those of standard binning, albeit to a lesser degree. While the wider width binning methods produce MRCs that are close to unity for vibrationally elastic collisions, they diverge from unity for vibrationally inelastic collisions. Furthermore, the wider the effective width of the binning function, the more likely the MRCs are to deviate from unity in areas where the differential cross section is non-linear. From these considerations, **we conclude that the effective width of the binning function is the main factor in determining whether binning methods are consistently microscopically reversible**.

Additionally, we have found that certain processes are more amenable to microscopic

reversibility than others. **We find that as long as the differential cross section is either symmetrical or linear within the standard bin of the final quantum state, microscopic reversibility will be satisfied for all binning methods.** Now that we have examined both microscopic reversibility and empirical agreement for our QCT methods, we provide a summary of our results in the following chapter.

Chapter 6

Summary and Discussion of Results

In this study, we have examined the agreement between quasiclassical and quantum mechanical cross sections for the $Li_2(v_i = 0, j_i = 18)$ + Ne scattering system. We examined the system in two regimes: the high energy regime where we expected quantum mechanical effects such as interference and tunneling to be negligible, and the threshold regime, where we believed quantum effects would be important. However, even at high energy, it is difficult to simulate our system using the QCT, because classical mechanics does not force the molecule to inhabit discrete bound states at the end of the collision. As a result we have to assign a continuous distribution of classical rovibrational actions to discrete quantum numbers in order to calculate cross sections. This process known as binning.

In this study, we analyzed the various different binning methodologies, which can effectively be sorted into three groups. As a tool for comparison, we used the standard binning method, which calculates the collision cross sections by rounding the final rovibrational actions towards the nearest allowed quantum states. As computational power has grown, this tool has been phased out due to the fact that the rounding process changes the energy of the final rovibrational state.

The second group of methodologies that we analyzed is what we have referred to as narrow-width binning. These methods involve using a narrow-width binning function in order to only effectively sample trajectories that make allowed quantum transitions. We usually implement this method using a gaussian binning function, which weights the contribution of each trajectory towards the final quantum state by a narrow-width-gaussian centered at the final quantum number [Bonnet and Rayez [11]]. The FWHM of this gaussian is chosen so that the value of the cross section converges to the value it would predict in the case of zero width. Additionally, we implement narrow-width binning by calculating vibrational and rotational differential cross sections. We do this by binning our classical trajectories, not only at the allowed quantum numbers, but at a variety of classical actions in between. When we do this for enough classical actions, we are able to interpolate a function that models the differential cross section. We show that evaluating the differential cross section at an allowed quantum state and multiplying by the standard bin width is equivalent to calculating the collision cross section using delta-function binning.

The final methodology archetype is the symmetrical windowing method, which allows the initial quantum number to correspond a distribution of initial classical actions.

After calculating the final classical actions, the trajectories are binned using the same distribution function that they were sampled with [Cotton and Miller [14]].

We began our study by analyzing vibrationally elastic collisions at a total energy of 2500 cm^{-1}, where we expected wave effects to be small. We found that the best way to produce good agreement with quantum mechanical results for vibrationally elastic collisions, was to use standard binning on the vibrational actions and a narrow-width binning method on the rotational actions. When we attempted to use a narrow-width binning method on vibration as well as rotation, we found that the predicted cross sections were an order of magnitude too large. Furthermore, we found that the cross sections grew continuously as we shrunk the FWHM of the vibrational gaussian, until the error rendered our data useless.

For vibrationally inelastic collisions, we found that using a narrow width binning method in both vibration and rotation better predicts the total vibrationally inelastic cross section. However, we did not find that narrow-width binning methods significantly improve the distribution of vibrationally inelastic cross sections as a function of rotational quantum number.

Later in the study, we attempted to gauge how classically correct these methods are by testing them for time-reversal symmetry. We found that in order to ensure microscopic reversibility, binning must be done over a narrow-width-distribution, in order to only utilize classical trajectories that undergo full quantum mechanical transitions. **Since we found that narrow-width binning methods obey time reversal symmetry and generally agree better with quantum mechanics, we believe that they are the best available analytic tool for calculating**

classical cross sections away from threshold. The lone exception to this rule occurs when the vibrational differential cross section is narrowly peaked about the final quantum number. In this case, the cross section grows rapidly as the bin width is shrunk, and the narrow-width cross section is inaccurate. However, this is not a serious practical issue, as we have argued that standard binning will produce good empirical agreement with quantum mechanics and satisfy time-reversal symmetry in this case.

As we moved closer towards the threshold for vibrational excitation, the quantum mechanical and classical cross sections diverged even further due to tunneling effects. In order to confront this problem, we tested the symmetrical windowing method, which has been shown by Cotton and Miller to improve the energy dependence of the threshold in collinear H + H_2 reactions [Cotton and Miller [14]]. Unfortunately, we found that the symmetrical windowing method was unable to recover the threshold behavior of quantum mechanics for most rovibrational transitions. Furthermore, we found that standard binning is just as effective at lowering the threshold energy, as it also allows for trajectories to make vibrational transitions without gaining all of the necessary classical energy, i.e. trajectories that satisfy, $\Delta v_c < 1,\ \Delta v_f = 1$. When we tested the symmetrical windowing method for microscopic reversibility, we found that it violates time-reversal symmetry in a similar way to standard binning. In light of these considerations, **we see no theoretical advantage of the symmetrical windowing methods over standard binning. While both methods are able to recover some of the threshold behavior of quantum mechanics by allowing $\Delta v_c < 1$ trajectories, they pay the consequences in their failure**

to satisfy microscopic reversibility.

We advocate that when applying any of these QCT methods to novel systems, that one looks closely at the differential cross sections. Through a qualitative analysis of the shapes of the differential cross section, we are already able to tell whether the process will be microscopically reversible for the wider-width standard binning and symmetrical windowing methods, and whether these wider-width methods will produce smaller or larger collision cross sections than the narrow width methods. We leave this table for reference

distribution shape	wide-width MRC = 1?	$\frac{\text{wide-width binning}}{\text{narrow-width binning}}$
peaked distribution	yes	< 1
negative power law	no	> 1
linear	yes	1
two drop	no	not studied

6.1 Future Studies

In this study, we have shown that the classically correct way of describing the cross-section of a $Li_2 + Ne$ rovibrational transition is through doubling the value of its classical differential cross section. This idea can easily be generalized to higher dimensional systems by replacing the 2 in our equality with the 'volume' of a quantum number separation in all of the degrees of freedom that are binned. Furthermore, we have shown that narrow-width binning methods are able to improve agreement

with quantum mechanics and ensure that classical time reversal symmetry is satisfied for the Li_2 + Ne system. We invite future studies to test these conclusions on other systems with limited wave effects, to ensure that they are not specific to three-body systems or inelastic scattering. Finally, we found that there were areas where we were unable to calculate the vibrational differential cross section due to a thick density of trajectories around the final quantum number. We believe that a more through examination of this issue, including understanding when it will arise and how it can be remedied, would be useful for clarifying when it is appropriate to use narrow-width binning.

We have found that the symmetrical windowing method is not microscopically reversible for our Li_2 + Ne system. However, we speculate that it may be possible to create a method that samples and bins over a non-zero width, that is also microscopically reversible. In order to do so, one would have to ensure that the sampled distribution of states around v_f was always equal to the product of the binning curve and the differential cross section, a daunting task.

We have done a systematic study on the effect of binning on the collision cross sections for inelastic scattering in the Li_2 + Ne system. While we are happy to find modifications to the QCT that improve agreement with quantum mechanics in our system, we hope that we have provided a method of inquiry that will help others effectively carry out the quasiclassical method in their systems. We encourage others to focus more on this problem, as accurate classical calculations can provide an intuitive, quick way of understanding collision systems that quantum mechanics cannot.

Bibliography

[1] L Banares, FJ Aoiz, P Honvault, B Bussery-Honvault, and J-M Launay. Quantum mechanical and quasi-classical trajectory study of the C (^{1}D)+ H_2 reaction dynamics. *The Journal of Chemical Physics*, 118(2):565–568, 2003.

[2] Nadia Balucani, Giovanni Capozza, Laura Cartechini, Astrid Bergeat, Rolf Bobbenkamp, Piergiorgio Casavecchia, F Javier Aoiz, Luis Banares, Pascal Honvault, Béatrice Bussery-Honvault, et al. Dynamics of the insertion reaction C(^{1}D) + H_2: A comparison of crossed molecular beam experiments with quasiclassical trajectory and quantum mechanical scattering calculations. *Physical Chemistry Chemical Physics*, 6(21):4957–4967, 2004.

[3] Nadia Balucani, Piergiorgio Casavecchia, Luis Banares, F Javier Aoiz, Tomas Gonzalez-Lezana, Pascal Honvault, and Jean-Michel Launay. Experimental and theoretical differential cross sections for the N(^{2}D)+ H_2 reaction. *The Journal of Physical Chemistry A*, 110(2):817–829, 2006.

[4] Gábor Czakó and Joel M Bowman. Quasiclassical trajectory calculations of correlated product distributions for the F+ CHD_3 (v_1= 0, 1) reactions using an

ab initio potential energy surface. *The Journal of Chemical Physics*, 131(24): 244302, 2009.

[5] C Díaz, JK Vincent, GP Krishnamohan, RA Olsen, GJ Kroes, K Honkala, and Jens Kehlet Nørskov. Reactive and nonreactive scattering of n_2 from Ru (0001): a six-dimensional adiabatic study. *The Journal of Chemical Physics*, 125(11): 114706, 2006.

[6] W.R. Gentry. In R.B. Bernstein, editor, *Atom-Molecule Collision Theory: A Guide for the Experimentalist*. Plenum, New York, 1979.

[7] Kristin M Burgess. *Implementation of a quasiclassical model for atom-diatom collisions*. PhD thesis, Wesleyan University, 1997.

[8] N Smith. *The Journal of Chemical Physics*, 1987.

[9] MH Alexander, A Berning, A Degli Esposti, A Joerg, A Kliesch, and H-J Werner. Theoretical studies of collision-induced energy transfer in electronically excited states. *Berichte der Bunsengesellschaft für physikalische Chemie*, 94(11):1253–1262, 1990.

[10] Brian Stewart, Peter D Magill, and David E Pritchard. Quasi-resonant vibration-rotation transfer in inelastic Li_2^* - Ne collisions. *The Journal of Physical Chemistry A*, 104(45):10565–10575, 2000.

[11] L Bonnet and JC Rayez. Quasiclassical trajectory method for molecular scattering processes: necessity of a weighted binning approach. *Chemical physics letters*, 277(1):183–190, 1997.

[12] AJC Varandas. Trajectory binning scheme and non-active treatment of zero-point energy leakage in quasi-classical dynamics. *Chemical physics letters*, 439 (4):386–392, 2007.

[13] Laurent Bonnet and Joaquin Espinosa-Garcia. The method of gaussian weighted trajectories. v. on the 1GB procedure for polyatomic processes. *The Journal of Chemical Physics*, 133(16):164108, 2010.

[14] Stephen J Cotton and William H Miller. Symmetrical windowing for quantum states in quasi-classical trajectory simulations. *The Journal of Physical Chemistry A*, 117(32):7190–7194, 2013.

[15] M.D. Pattengill. In R.B. Bernstein, editor, *Atom-Molecule Collision Theory: A Guide for the Experimentalist*. Plenum, New York, 1979.

[16] Laurent Bonnet and Jean-Claude Rayez. Gaussian weighting in the quasiclassical trajectory method. *Chemical Physics Letters*, 397(1):106–109, 2004.

[17] Estela Carmona-Novillo, Tomás González-Lezana, Octavio Roncero, Pascal Honvault, Jean-Michel Launay, Niyazi Bulut, F Javier Aoiz, Luis Bañares, Alexandre Trottier, and Eckart Wrede. On the dynamics of the H + D_2 (v= 0, j= 0) $\rightarrow$ HD + D^+ reaction: A comparison between theory and experiment. *The Journal of Chemical Physics*, 128(1):014304, 2008.

[18] L Banares, FJ Aoiz, P Honvault, and J-M Launay. Dynamics of the S(^{1}D)+ H_2 insertion reaction: a combined quantum mechanical and quasiclassical trajectory study. *The Journal of Physical Chemistry A*, 108(9):1616–1628, 2004.

[19] Tiao Xie, Joel Bowman, JW Duff, M Braunstein, and B Ramachandran. Quantum and quasiclassical studies of the O (3p)+ HCl → OH+ Cl (2P) reaction using benchmark potential surfaces. *The Journal of Chemical Physics*, 122(1): 014301, 2005.

[20] M Jorfi, P Honvault, Ph Halvick, SY Lin, and H Guo. Quasiclassical trajectory scattering calculations for the OH + O → H+ O_2 reaction: Cross sections and rate constants. *Chemical Physics Letters*, 462(1):53–57, 2008.

[21] Wenqin Zhang, Shulin Cong, Cuihua Zhang, Xuesong Xu, and Maodu Chen. Theoretical study of dynamics for the abstraction reaction H' + HBr (v= 0, j= 0) → H + Br. *The Journal of Physical Chemistry A*, 113(16):4192–4197, 2009.

[22] Sanjay Kumar, N Sathyamurthy, and Ramakrishna Ramaswamy. Overcoming the zero-point dilemma in quasiclassical trajectories:(He, H_2^+) as a test case. *The Journal of Chemical Physics*, 103(14):6021–6028, 1995.

[23] ME Mandy and PG Martin. Quasiclassical integral cross sections for H + H_2 (0, j= 0, 2) → H_2 (1, j' = 1, 3, 5) + H. *The Journal of Chemical Physics*, 97 (1):265–269, 1992.

[24] AJC Varandas. A novel non-active model to account for the leak of zero-point energy in trajectory calculations. application to H + O_2 reaction near threshold. *Chemical physics letters*, 225(1):18–27, 1994.

[25] Brian A Stewart, Troy N Stephens, Barbara A Lawrence, and George C McBane. Rovibrational energy transfer in Ne - Li_2 ($A1\Sigma_u^+$, v = 0): Comparison

of experimental data and results from classical and quantum calculations. *The Journal of Physical Chemistry A*, 114(36):9875–9885, 2010.

[26] JM Hutson and S Green. Molscat computer code, version 14. *Collaborative Computational Project*, (6), 1994.

[27] G McBane and P Valiron. Pmp molscat, a parallel version of molscat, version 14.

[28] Richard C Tolman. The principle of microscopic reversibility. *Proceedings of the National Academy of Sciences of the United States of America*, 11(7):436, 1925.

[29] JC Polanyi and JL Schreiber. Physical chemistry- an advanced treatise. In *Kinetics of gas reactions*, volume 6, pages 383–487. Academic Press New York, 1974.

[30] Laurent Bonnet. Classical dynamics of chemical reactions in a quantum spirit. *International Reviews in Physical Chemistry*, 32(2):171–228, 2013.